

Hydration Dynamics and IR Spectroscopy of 4-Fluorophenol

Seyedeh Maryam Salehi, Silvan Käser, Kai Töpfer,[†] Polydefkis Diamantis,[‡] Rolf Pfister, Peter Hamm,[¶] Ursula Röthlisberger,[§] and Markus Meuwly^{*,†}

[†]*Department of Chemistry, University of Basel, Klingelbergstrasse 80 , CH-4056 Basel, Switzerland.*

[‡]*Laboratory of Computational Chemistry and Biochemistry, Institute of Chemical Sciences and Engineering, École Polytechnique Fédérale de Lausanne, CH-1015 Lausanne, Switzerland.*

[¶]*Department of Chemistry, University of Zurich*

[§]*Laboratory of Computational Chemistry and Biochemistry, Institute of Chemical Sciences and Engineering, École Polytechnique Fédérale de Lausanne (EPFL), CH-1015 Lausanne, Switzerland.*

E-mail: m.meuwly@unibas.ch

Abstract

Halogenated groups are relevant in pharmaceutical applications and potentially useful spectroscopic probes for infrared spectroscopy. In this work, the structural dynamics and infrared spectroscopy of *para*-fluorophenol (F-PhOH) and phenol (PhOH) is investigated in the gas phase and in water using a combination of experiment and molecular dynamics (MD) simulations. The gas phase and solvent dynamics around F-PhOH and PhOH is characterized from atomistic simulations using empirical energy functions with point charges or multipoles for the electrostatics, Machine-Learning (ML) based parametrization and with full *ab initio* (QM) and mixed Quantum Mechanical/Molecular Mechanics (QM/MM) simulations with a particular focus on the CF- and OH-stretch region. The CF-stretch band is heavily mixed with other modes whereas the OH-stretch in solution displays a characteristic high-frequency peak around 3600 cm^{-1} most likely associated with the -OH group of PhOH and F-PhOH together with a characteristic progression below 3000 cm^{-1} due to coupling with water modes which is also reproduced by several of the simulations. Solvent and radial distribution functions indicate that the CF-site is largely hydrophobic except for simulations using point charges which renders them unsuited for correctly describing hydration and dynamics around fluorinated sites.

Introduction

Fluorination - and halogenation in general - are common chemical modifications for pharmaceuticals. Approximately 20 % of all small molecule drugs used in medicinal chemistry contain $X = \text{F}, \text{Cl}, \text{Br}, \text{or I}$ or a combination thereof. Among these compounds halogenated phenyl rings constitute an important class.¹ Because of the directionality of the interaction along the C-X bond due to the sigma hole, halogenation has emerged as one of the essential chemical modifications in medicinal materials,²⁻⁴ and supramolecular chemistry.^{5,6} By changing the halogen atom, the interactions with the environment can be tuned and

the hydrophobicity around the modification site can be modulated.^{3,7-12} The importance of halogenation as a fundamental concept in medicinal chemistry is highlighted by the improved binding affinities of several ligands towards their receptors.^{13,14} Recently, halogenation has also been employed in the context of protein modifications, such as for insulin, to fine-tune thermodynamic stability and affinity to the insulin receptor.¹⁵

A halogen bond “[..]occurs when there is evidence of a net attractive interaction between an electrophilic region associated with a halogen atom in a molecular entity and a nucleophilic region in another, or the same, molecular entity.”¹⁶ Hence, halogen atoms act as electrophiles and can form an attractive interaction with a nucleophilic counterpart. Based on the analysis of the molecular surface electrostatic potential (ESP),¹⁷ the “halogen bond” was also associated with a “ σ -hole bond”¹⁸ which is a noncovalent interaction between a covalently-bonded halogen atom X and a negative site, e.g. a lone pair of a Lewis base or an anion.¹⁷ Such a “bond” involves a region of positive electrostatic potential, i.e. the σ -hole, and as an extension of one of the covalent bonds to the atom. The σ -hole arises as a consequence of the anisotropy of the ESP around the halogen atom. The strengths of the interactions generally correlate well with the magnitudes of the positive and negative electrostatic potentials of the σ -hole and the negative site. As fluorine has the largest electronegativity and the lowest polarizability, for some time it was in fact assumed that there is no σ -hole and that therefore fluorine is not involved in halogen bonding at all.^{17,19,20} However it is now well established that it can have a positive σ -hole and form halogen bonds when it is linked to strongly electron-withdrawing groups including Cl, Br, and I.^{21,22} Moreover, there is also experimental evidence for fluorine engaging in halogen bonding.²³

Introducing a fluorine atom into organic molecules can cause major changes in the physico-chemical properties such as solubility, chemical reactivity and biological activity compared to non-fluorinated analogues.²⁴ In particular, fluorine often replaces hydrogen in organic

molecules but the size and stereoelectronic influences of the two atoms (hydrogen vs. fluorine) are quite different albeit it is often regarded as isosteric substitution.⁴ In bio-inorganic and medicinal chemistry, the formation of intermolecular O–H/F–C and N–H/F–C hydrogen bridges was assumed to be important in binding fluorinated compounds to enzyme active sites.²⁵ Such interactions affect enzyme ligand binding affinity, selectively coupled with the changes in pharmaco-kinetic properties by fluorine substitution.^{10,24} The effects of fluorine substitution on the related pharmaco-kinetic properties like lipophilicity, volatility, solubility, hydrogen bonding and steric effects affect the resulting compound binding, absorption, transport and hence the related biological activity.²⁶

A variety of functional groups, including C–H, C–OH, C=O, and C≡N, have utilized the C–F bond as a bioisostere.²⁷ However, it is difficult to generalize the relative ability of fluorine to act similar to a hydrogen or hydroxy group, and different factors must be considered in each case. The van der Waals radius of fluorine (1.47 Å) lies between that of oxygen (1.57 Å) and hydrogen (1.2 Å) and as it is the element with the highest electronegativity, the C–F bond is almost identical to C–OH in terms of bond length and polarity. Despite its three electron pairs, the C–F bond interacts more weakly with the environment compared to an oxygen atom and is better described as “weakly polar” rather than “hydrogen bonding”.^{27,28} In pharmacological applications the replacement H→F is often considered to avoid metabolic transformation due to the high stability of the CF bond. Examples are drugs interacting with P450 for which fluorination has been widely used to block metabolic transformations.²⁷

Given the different qualitative characterizations outlined so far, a more molecularly refined picture of the energetics and dynamics involving fluorinated model compounds will be valuable. The present work considers hydrated fluoro-phenol (F-PhOH) as a typical representative. Using linear infrared spectroscopy together with computational characterizations at different levels of theory the structural dynamics and spectroscopy of F-PhOH is charac-

terized. The computations use advanced empirical force fields including multipolar interactions, a machine-learned, neural network-based representation of a full-dimensional PES, mixed quantum mechanics/molecular mechanics and *ab initio* MD simulation techniques. The measured data from infrared spectroscopy can be directly compared with the computational results. Also, the solvent dynamics is investigated based on frequency fluctuation correlation and spatial distribution functions. In this article, first, the methods are described followed by the results for the spectroscopy of the -CF and -OH from experiments and simulations. Then, the solvent structure is analyzed from radial distribution functions and from 2-dimensional solvent distributions and finally, conclusions are drawn.

Methods

Classical Molecular Dynamics Simulations

All classical MD simulations were performed with CHARMM.²⁹ The bonded parameters are based on CGenFF³⁰ except for the CF and OH bond for which a Morse potential was used to describe their anharmonicity. To that end, a scan along the CF bond was performed at the MP2/aug-cc-pVTZ level starting from an optimized structure of F-PhOH at this level of theory. The energy of 49 points was computed on a grid ranging from $r = 0.75$ Å to $r = 5.55$ Å in increments of 0.1 Å. Then, the energies were fitted to a Morse potential $V(r) = D_0[1 - \exp(-\beta(r - r_0))]^2$ which yields parameters $D_0 = 136.316$ kcal/mol, $r_0 = 1.349$ Å, and $\beta = 1.603$ Å⁻¹. For the OH bond the calculated Morse parameters are $D_0 = 120.234$ kcal/mol, $r_0 = 0.971$ Å, and $\beta = 2.088$ Å⁻¹. To realistically describe the electrostatic interactions, a multipolar (MTP)³¹⁻³⁴ model was also used with MTPs on all heavy atoms up to quadrupoles and point charges for all hydrogen atoms. These parameters were fitted to the electrostatic potential using a fitting environment,³⁵ see Tables S1 to S3.

Simulations of F-PhOH and PhOH were carried out in a cubic box of 30^3 \AA^3 (28^3 \AA^3 for simulations with the NN-PES, see below) using TIP3P³⁶ water molecules. Minimization, heating, and equilibration procedures for 40 ps were employed to prepare the system. Production simulations of 5 ns were run in the *NVE* ensemble at 300 K using a Velocity Verlet.³⁷ The time step was $\Delta t = 1 \text{ fs}$ and every 5 snapshot was recorded. Lennard-Jones interactions were computed with a 12 \AA cutoff switched at 10 \AA .³⁸ The electrostatic interactions for the monopoles (point charges) are treated using Particle-Mesh Ewald³⁹ (PME) with grid size spacing of 1 \AA , characteristic reciprocal length $\kappa = 0.32 \text{ \AA}^{-1}$, and interpolation order 6. All bonds involving hydrogen atoms are constrained via the SHAKE algorithm.^{40,41} Additional MD simulations were also carried out for PhOH in water with the same setup that was used for F-PhOH in order to directly compare their spectroscopy and solvent structure.

For the simulations with the NN-based PES (see below) the atomic simulation environment (ASE) was used.⁴² The van-der-Waals interactions were those from the CGenFF³⁰ parametrization and the fluctuating charges are from the PhysNet representation, see below. For both terms interactions the cutoff distance is at 14 \AA and switched between 13 to 14 \AA . To avoid artifacts of the electrostatic Coulomb force in the cutoff range, the Coulomb force at the distance of 14 \AA was shifted to zero in accordance to the shifted forces method.⁴³ In the gas phase 1000 trajectories, each 200 ps in length, are run to obtain an ensemble average. The *NVE* simulations are run at 300 K initialized from random momenta corresponding to a Maxwell-Boltzmann distribution, with a time step of 0.5 fs, equilibrated for 50 ps and propagated for 200 ps. Simulations in solution *NVT* using Langevin⁴⁴ thermostat at 300 K are performed for 20 trajectories of 100 ps each with a time step of 0.2 fs to obtain a total of 2 ns for PhOH and F-PhOH in solution, respectively. The IR spectra are then calculated from the dipole-dipole moment autocorrelation function⁴⁵⁻⁴⁷ and averaged over all 1000 trajectories.

Instantaneous Normal Mode Analysis

From the production simulation, 10^6 snapshots were taken as a time-ordered series for computing the frequency fluctuation correlation function (FFCF). The FFCF was determined from instantaneous harmonic vibrational frequencies based on a normal mode analysis. Such instantaneous normal modes (INM) are obtained by minimizing F-PhOH while keeping the surrounding solvent frozen. Next, normal modes were calculated using CHARMM for 5 modes (ν_1 to ν_5 in ascending order) between 1100 to 1400 cm^{-1} in terms of participation ratio of CF stretch in that particular mode. In a separate analysis step, the participation ratios of the CF, CO, and CH stretch and the COH bending coordinates to these 5 normal modes were determined.

Frequency Fluctuation Correlation Function and Lineshape

From the INMs the frequency trajectory $\omega_i(t)$ and the FFCF, $\langle \delta\omega(0)\delta\omega(t) \rangle$ was computed. Here, $\delta\omega(t) = \omega(t) - \langle \omega(t) \rangle$ and $\langle \omega(t) \rangle$ is the ensemble average of the transition frequency. From the FFCF the line shape function

$$g(t) = \int_0^t \int_0^{\tau'} \langle \delta\omega(\tau'') \delta\omega(0) \rangle d\tau'' d\tau'. \quad (1)$$

is determined within the cumulant approximation. To compute $g(t)$, the FFCF is numerically integrated using the trapezoidal rule and the 1D-IR spectrum is calculated from⁴⁸

$$I(\omega) = 2\Re \int_0^\infty e^{i(\omega - \langle \omega \rangle)t} e^{-g(t)} e^{-\frac{t\alpha}{2T_1}} dt \quad (2)$$

where $\langle \omega \rangle$ is the average transition frequency obtained from the distribution, $T_1 = 1.2$ ps⁴⁹ is the vibrational relaxation time and $\alpha = 0.5$ is a phenomenological factor to account for lifetime broadening.⁴⁸

From the FFCF, the decay time is determined by fitting the FFCF to a general expression⁵⁰

$$\langle \delta\omega(t)\delta\omega(0) \rangle = \sum_{i=2}^n a_i e^{-t/\tau_i} + \Delta_0 \quad (3)$$

where a_i , τ_i and Δ_0 are fitting parameters. The decay times τ_i from the fits characterize the time scale of the solvent fluctuations. The absence of a minimum at short times ($\tau \sim 0.02$ ps) indicates that the interaction between F and environment is weak compare with situation in F-ACN or N_3^- .^{49,51} The decay times τ_i of the FFCF reflect the characteristic time-scale of the solvent fluctuations to which the solute degrees of freedom are coupled. In all cases the FFCFs were fitted to an expression containing two decay times using an automated curve fitting tool from the SciPy library.⁵²

Full *Ab Initio* (QM) and Mixed Quantum Mechanical/Molecular Mechanics (QM/MM) Simulations

Full QM Simulations: The QM system was comprised of F-PhOH and 117 water molecules in a (15.41 Å ,15.44 Å ,15.46 Å) periodic box initially equilibrated classically at 300 K and 1 atm using CHARMM. The full QM equilibration and production phases lasted for 12.5 ps and 20.4 ps respectively. For the gas phase simulation, the total equilibration and production times were 23.0 ps and 28.1 ps, respectively. For the latter, the initial translations and rotations of the center of mass were removed.

For both the gas phase and the condensed phase systems, the full QM simulation protocol consisted of (i) an equilibration of the system at 300 K first with Born-Oppenheimer (BO) MD and then with Car-Parrinello (CP) MD,⁵³ and (ii) a production phase in the micro-canonical (*NVE*) ensemble. The respective time steps for BO and CP MD were 10 and 2 atomic units (a.u.), respectively. In CP MD, the fictitious electron mass was equal to 400 a.u.

In the production phase, frames were saved every 10 a.u., corresponding to a time interval of approximately 0.48 fs.

Density Functional Theory (DFT)-based *ab initio* MD simulations of F-PhOH in gas phase and in aqueous solution were carried out using the CPMD code⁵⁴ using the BLYP functional for the exchange and correlation energies^{55,56} with the addition of Dispersion-Corrected Atom-Centered Potentials (DCACPs)⁵⁷⁻⁵⁹ for the description of dispersion forces.

Norm-conserving Martins-Trouiller pseudopotentials⁶⁰ were used in combination with a plane wave basis with a 175 Rydberg kinetic energy cutoff for the expansion of the single-particle wavefunctions. The latter value was selected because it reproduces a converged equilibrium C-F bond distance at the BLYP-DCACP level of 1.35 Å for F-PhOH in gas phase, which is in good agreement with values obtained at the MP2/6-311++G(df,pd) (1.34 Å) and B3LYP/6-311++G(df,pd) (1.35 Å) levels, respectively.⁶¹

Mixed QM/MM Simulations: Two QM/MM MD simulations were carried out for F-PhOH and PhOH in water, respectively, using the QM/MM interface of CPMD with the Gromos code⁶² and the coupling scheme developed by Rothlisberger and coworkers.⁶³⁻⁶⁵ The two systems were comprised of the solute (F-PhOH or PhOH), and 331 and 311 water molecules, respectively. The system size was selected so that a direct comparison with the full QM simulation of F-PhOH in water can be made, and assess the impact of quantum description of the solvent including polarization effects on the geometric and spectral properties of F-PhOH.

The systems were first equilibrated classically, using AMBER18.⁶⁶ F-PhOH and PhOH were modelled with the GAFF2 force field,^{67,68} while the TIP3P model was used for water. Following an initial minimization, the two systems were equilibrated in the isothermal-isobaric (*NPT*) (300 K, 1 atm) ensemble with the Berendsen barostat⁶⁹ and Langevin dynamics⁴⁴ for

pressure and temperature control respectively, followed by simulations in the NVT ensemble with Langevin dynamics, for a total of 100 ns. A time step of 2 fs was employed. In view of the small periodic box size, a reduced real space cutoff of 7 Å was used for the nonbonded interactions.

In both systems, the solute was treated at the QM level and the solvent at the classical (MM) level. The QM setup, and the simulation time step were the same as described above for the full QM simulations. The QM/MM MD simulation protocol was also similar to the one described for the full QM simulation, apart from the use of two separate Nosé-Hoover thermostats for the QM and MM parts respectively, during the equilibration with BO and CP MD. For the F-PhOH system, the equilibration and production runs lasted 10.1 ps and 35.9 ps respectively, while for the PhOH system they lasted 12.6 ps and 25.0 ps, respectively. During the production phase, frames were saved with the same frequency as in the full QM simulations (0.48 fs).

Machine-Learned Potential Energy Surface (PES)

To validate in particular the PC- and MTP-based simulations using an empirical force field a complementary model based on a machine-learned PES was also pursued. For this PhysNet,⁷⁰ a deep neural network (NN) of the message passing type,⁷¹ was used to obtain a representation of the potential energy for both PhOH and F-PhOH. PhysNet uses Cartesian coordinates and nuclear charges to learn an atomic descriptor for the prediction of energies, forces, partial charges and molecular dipole moments to describe chemical systems and their properties, such as infrared spectra.

PhysNet was trained on *ab initio* energies, forces and dipole moments calculated at the MP2/6-31G(d,p) level of theory using Molpro⁷² according to the protocol reported in Ref.⁷⁰

The reference data, containing different geometries for both molecules, is generated from MD simulations at 50, 300 and 1000 K using CHARMM force field (5000 geometries each yielding a total of 30000 geometries) and extended with geometries obtained from normal mode sampling⁷³ at temperatures between 10 and 2000 K (6600 geometries for each molecule). The complete data set thus contains 43200 PhOH and F-PhOH structures. The performance of the PhysNet PES is reported in Figure S1 which shows the correlation between the reference MP2 and the PhysNet energies for a test set of 3700 randomly selected points with $R^2 = 0.9999$ and an RMSE of 0.0037 eV. Simulations with PhysNet for the solute and an empirical water model are subsequently referred to as ML/MM MD.

Experimental Infrared Spectroscopy

Experimental spectra of PhOH and F-PhOH in water have been measured in attenuated total reflection (ATR) geometry using a home-constructed ZnSe prism in a Bruker Tensor 27 FT-IR spectrometer. Identical concentrations of 0.76 M have been used for both samples, which is the saturation limit for F-PhOH. As a background spectrum, pure water has been measured as well and subtracted from the PhOH and F-PhOH spectra. The subtraction procedure is deemed reliable in the shown spectra, with the exception of the range between $\approx 3100 \text{ cm}^{-1}$ to 3500 cm^{-1} , where the very strong OH stretch vibration dominates. In fact, in this range a dispersion-shaped response is observed, which is attributed to the effect the samples have on the water spectrum, i.e., a shift to somewhat higher frequencies due to overall weaker water-water hydrogen bonds.

Results

Gas Phase Spectra

First, the performance of the PC- and MTP-based empirical force fields, of PhysNet, and of the DFT-BLYP/DCACP based *ab initio* MD simulations was assessed for F-PhOH in the gas phase. For this, MD simulations of F-PhOH in the gas phase were carried out and the power and infrared spectra were determined and compared with experiments.

Figure 1 reports the infrared and CF-/OH-power spectra of F-PhOH from simulations with the experimental FT-IR spectrum⁶¹ from 1100 to 1400 cm^{-1} and between 2600 and 4000 cm^{-1} , respectively. For clarity, the left hand column shows the low-frequency vibrations whereas the right hand column is for the -OH-stretch region. The experiments were carried out in CCl_4 solvent and the spectral lines have a full width at half maximum of $\sim 10 \text{ cm}^{-1}$. As an indication for the solvent-induced shift incurred, for PhOH in CCl_4 the CO stretch is found at 1257 cm^{-1} which amounts to a red shift of $\sim -5 \text{ cm}^{-1}$ compared with the gas-phase frequency of 1261.7 cm^{-1} .^{74,75} Hence, CCl_4 -induced shifts for F-PhOH are expected to be a few wavenumbers as well. To the best of our knowledge, no gas-phase spectra are available for F-PhOH. Hence, the frequencies for F-PhOH measured in CCl_4 are used *in lieu* of gas phase data.

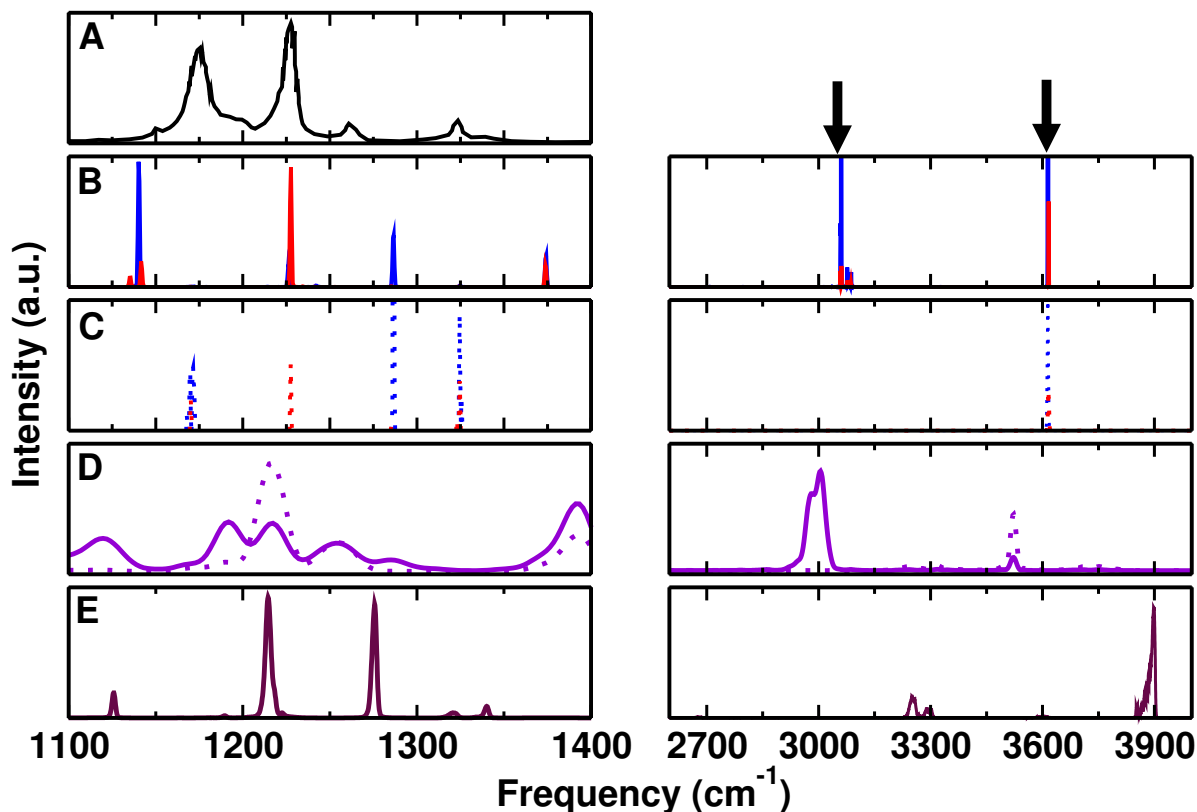


Figure 1: Comparison of experimental (in CCl_4) and computed (in the gas phase) spectra for F-PhOH in the range of (1100-1400 cm^{-1}) and (2600 to 4000 cm^{-1}). Panel A: experimental (black) spectrum in CCl_4 from Ref.⁶¹ extracted using g3data.⁷⁶ The arrows in the right hand column refer to the experimental frequencies for the CH and OH stretches.⁶¹ Panels B and C: IR from the Fourier transform of the total dipole moment correlation function and CF/OH power spectra from PC (blue) and MTP (red) simulations for F-PhOH in the gas phase. Panel D: global (solid) and CF/OH (dotted) power spectrum in violet from QM simulations in the gas phase. Panel E: IR spectrum (maroon) obtained from ML/MM MD simulations.

The measured CF and CO stretching modes occur mainly at 1226 and 1262 cm^{-1} , respectively, while they couple to one another and potentially to other modes. According to the analysis^{61,75} (see Table 1), the CF stretch is coupled to the in plane bending of the ring and also the C-H bend while the CO stretch couples to the CC and CF stretching vibrations. Therefore, the CF stretch is intimately coupled with other modes and for that reason it is not possible to assign a local CF stretching mode to one particular frequency.

Table 1: Vibrational frequencies in cm^{-1} for PhOH (gas phase) and F-PhOH (in CCl_4) in the range of 1100-1400 cm^{-1} .^{61,74,75} The contributions (in terms of local deformations) to each vibrational mode indicate strong mixing and are those from the literature.^{61,74} The assignment of the bands has been made on the basis of the calculated potential energy distribution.^{61,77} Symbols ν and δ refer to stretching and bending modes, respectively.

PhOH	1150.7	1168.9	1176.5	1261.7	1343	3656	
	$\delta(\text{CH})$	$\delta(\text{CH})$	$\delta(\text{OH})$	$\nu(\text{CO})$	$\delta(\text{CH})$	$\nu(\text{OH})$	
	$\nu(\text{CC})$	$\nu(\text{CC})$	$\delta(\text{CH})$	$\delta(\text{CH})$	$\delta(\text{OH})$		
	$\delta(\text{OH})$	$\nu(\text{CC})$					
F-PhOH	1149	1174	1226	1262	1310	1323	3613
	$\delta(\text{CH})$	$\delta(\text{OH})$	$\nu(\text{CF})$	$\nu(\text{CO})$	$\delta(\text{CH})$	$\nu(\text{CC})$	$\nu(\text{OH})$
		$\nu(\text{CC})$	δring	$\nu(\text{CC})$	$\nu(\text{CC})$	$\delta(\text{OH})$	
		$\delta(\text{CH})$	$\delta(\text{CH})$	$\nu(\text{CF})$	$\delta(\text{CH})$		

For the force field simulations with PC and MTP the β -parameter of the CF-Morse potential (see Methods) was slightly adjusted to $\beta = 1.665 \text{ \AA}^{-1}$ to correctly describe the experimental spectrum in CCl_4 (Figure 1A), hence the favourable comparison with the IR spectra in Figure 1B. The CF power spectrum (Figure 1C left) clarifies that this mode couples strongly to other vibrations close in frequency for both, PC (blue) and MTP (red) force fields. The peak structure from the CF-power spectrum in Figure 1C left matches that from the experiment whereas for the IR spectrum in panel B this is only qualitatively the case. For the QM simulations in the gas phase (Figure 1D) the two main peaks of QM are at 1217 and 1256 cm^{-1} and appear to be shifted by 5 to 6 cm^{-1} with respect to experiments at 1222 and 1262 cm^{-1} which were recorded at $T = 300 \text{ K}$. Finally, MD simulations using the PhysNet representation of the MP2/6-31G(d,p) reference data the IR-spectrum in Figure 1E shows two strong peaks at 1215 cm^{-1} and 1276 cm^{-1} .

In the region of the OH-stretch vibration, the experimental spectrum for F-PhOH in CCl_4 reports a band at 3613 cm^{-1} (black arrow).⁶¹ This compares with 3614 cm^{-1} and 3616 cm^{-1} from PC and MTP simulations, respectively. Using PhysNet, the main peak in the gas phase is at 3889 cm^{-1} (harmonic frequency at 3882 cm^{-1} at the MP2/6-31G(d,p) level; corrected

frequency at 3655 cm^{-1} by multiplying with 0.94 for this level of theory⁷⁸) whereas the DFT-BLYP/DCACP QM simulations report the OH stretch at 3522 cm^{-1} , somewhat shifted to the blue and red, respectively, compared with experiment. Moreover, there are signatures in the infrared spectra due to the CH-stretch vibrations (black arrow) around $3035\text{-}3077\text{ cm}^{-1}$ which are also observed in the MD simulations. For PhysNet the corresponding peak is at 3256 cm^{-1} (3060 cm^{-1} after correction with a scaling factor of 0.94) whereas for QM at the DFT-BLYP/DCACP level the absorption is at 3006 cm^{-1} . The power spectra from the PC and MTP simulations (Figure 1C) confirm that the OH-stretch is a local mode.

In summary, the gas phase spectrum from finite- T MD simulations find comparable patterns for the frequencies in the $1100\text{ to }1400\text{ cm}^{-1}$ region when compared with experiment. It is also found that the CF stretch is coupled to other modes in this spectral range and no local mode for this motion can be assigned.

Spectroscopy and Dynamics of F-PhOH in Water

After assessing the energy functions considered in the present work, the spectroscopy of F-PhOH in solution is analyzed, see Figure 2. The experimentally measured spectrum from the present work is the black trace in Figure 2A with two prominent bands at 1201 and 1222 cm^{-1} in the CF-stretch region together with additional unresolved shoulders to higher energy, superimposed on a broad background extending from 1170 to 1270 cm^{-1} .

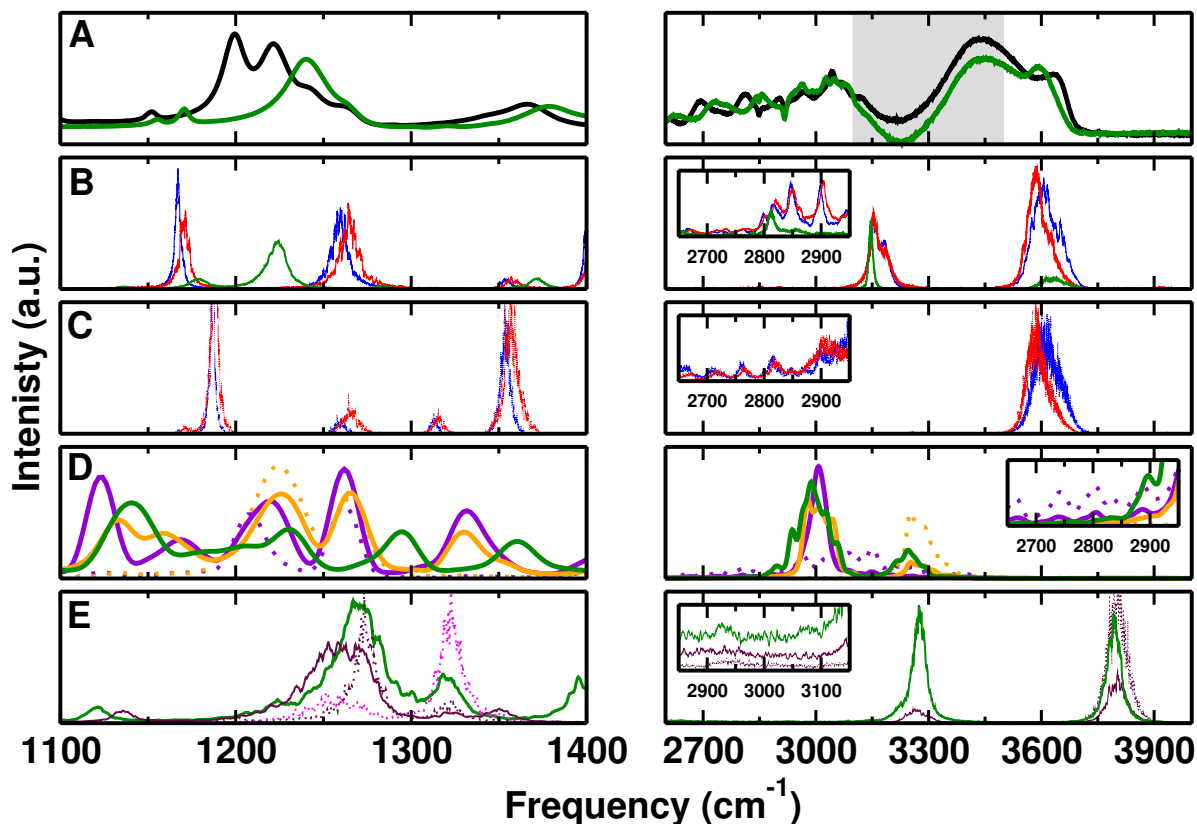


Figure 2: Comparison of experimental and computed spectra for F-PhOH and PhOH in solution for the ranges (1100-1400 cm^{-1}) and (2600 to 4000 cm^{-1}). Panel A: Measured spectrum for F-PhOH (black) and PhOH (green). The gray area from 3100 cm^{-1} to 3500 cm^{-1} is unreliable due to incomplete subtraction of the water background. Panel B: IR spectra for F-PhOH (PC (blue) and MTP (red)) and PhOH (MTP (green)). Panel C: CF/OH power spectra for F-PhOH from PC (blue) and MTP (red) simulations. Panel D: Global (solid) and CF/OH (dotted) power spectrum of the solute only (dotted) for F-PhOH (QM (violet) and QM/MM (orange)) and PhOH (QM/MM (green)). Panel E: IR (solid) and CF/OH (dotted) power spectrum for F-PhOH (maroon) and PhOH (green) from ML/MM simulations. The magenta dotted line is the CO power spectrum of F-PhOH. Insets in panels B to D show that the structured spectrum below 3000 cm^{-1} is also found from the simulations whereas with PhysNet this is less realistically captured compared with experiment.

The MTP/MD simulations for the CF power spectrum (Panel C) show two prominent peaks at 1187, and 1264 cm^{-1} which approximately line up with the features in the infrared spectrum (Panel B) but are displaced from those observed experimentally. The peak at 1171 cm^{-1} is red shifted compared to the double peak at 1201 and 1222 cm^{-1} of experimental spectrum while the peak at 1264 cm^{-1} is blue shifted or captured at the same position

compared to two additional experimental peaks at 1244 and 1264 cm^{-1} . Furthermore, the smaller peak at 1357 cm^{-1} is also red shifted compared to 1368 cm^{-1} from experiment. The corresponding infrared spectra in panel B align with the features at 1260 cm^{-1} but the signal at 1187 cm^{-1} from the power spectra has no oscillator strength in the infrared spectrum. Instead, a peak in the infrared appears at 1171 cm^{-1} .

The *ab initio* MD simulations in solution for the CF-power spectrum (Figure 2D solid violet) find two prominent bands at 1207 and 1262 cm^{-1} compared with band maxima at 1217 cm^{-1} with faint shoulders below 1200 cm^{-1} from gas-phase simulations, see Figure 1D. The two prominent bands are also found from QM/MM simulations (solid orange) with band maxima at 1225 and 1266 cm^{-1} . The CF-power spectra assign these features to CF-stretch involving motions and accounting for the scaling for BLYP calculations (~ 0.99 largely independent of basis set)⁷⁸ they shift to the red which is consistent with the experiments. Thus, the splitting between the two peaks decreases from 55 cm^{-1} for the full QM simulations to 41 cm^{-1} indicating the sensitivity of the solvent interactions and the resulting frequency shifts and splittings in this spectral range.

For ML/MM MD simulations a broad band is observed between 1220 to 1290 cm^{-1} in the IR spectrum which is blue shifted compared to the experiment. The CF-power spectrum with peak maximum at 1273 cm^{-1} (dotted maroon trace in Figure 1E) indicates that part of this broad IR-lineshape is due to CF-stretching motion. Moreover, the CO power spectrum has a first peak at 1250 cm^{-1} which contributes to the broad IR peak below 1300 cm^{-1} and a second, prominent peak at 1323 cm^{-1} , see Figure 1E. The overlapping peaks of the CF- and CO-power spectra indicate coupling between the two types of motion.

The high-frequency region of the experimental spectrum for solvated F-PhOH (Figure 2A) above and below 3000 cm^{-1} involves a broad absorption extending from ~ 2700 to 3100

cm^{-1} , a region between 3100 and 3500 cm^{-1} that is not reliable due to the dominating background from the OH stretch vibration of bulk water which can not be subtracted off completely (grey area in Figure 2A), and a high-frequency feature at 3643 cm^{-1} assigned to the free OH vibration presumably originating from F-PhOH but possibly also from H_2O . This latter assignment is less likely, though, as the same sharp peak appears for PhOH in solution but shifted to the red by $\sim 40 \text{ cm}^{-1}$. If the signal was due to water it is expected to occur at closer frequencies given the similarity of the solutes. Furthermore, experiments on hydrated PhOH with up to 49 water molecules find the water-OH-stretch vibration at $\sim 3700 \text{ cm}^{-1}$.⁷⁹ From simulations with PCs and MTPs the high frequency peak at 3607 cm^{-1} is consistent with experiment. Comparison with the spectrum for F-PhOH in CCl_4 and PhOH in the gas phase shows that this signal corresponds to the “free OH stretch” vibration, see Figure 1. Features at 3150 cm^{-1} in the infrared spectrum (Figure 1B) are due to the CH-stretch vibrations which could be brought into better agreement with experiment by slight reparametrization of the force constants. These features are not present in the OH-power spectra, Figure 1C, as expected which confirms the assignment to the CH-stretch vibration. The structured spectrum below 3000 cm^{-1} is present in both, the PC and MTP simulations, albeit with lower intensity.

For the full QM and QM/MM simulations the global power spectra (Figure 2D solid violet and orange) find a signal centered at 3000 cm^{-1} which is typical for the CH-stretch modes. At higher frequency ($\sim 3250 \text{ cm}^{-1}$) the OH-stretch vibration is located which is confirmed by the OH-power spectra (dotted violet and orange traces). However, no signal in the 3600 cm^{-1} region is present which suggests that the “free OH” signature in these simulations, expected around 3500 cm^{-1} from the QM gas phase simulations (Figure 1D), is absent.

Simulations with the PhysNet energy function primarily find the high frequency -OH stretch at 3803 cm^{-1} with broad, largely unstructured undulations below 3000 cm^{-1} . It is likely that

the MP2/6-31G(d,p) level is not sufficient for quantitatively describing the spectroscopy of F-PhOH. Accounting for a frequency scaling of 0.94 for harmonic frequencies⁷⁸ shifts all frequencies to the red which is more consistent with the experimentally determined spectra. Specifically, the 3800 cm^{-1} and 3280 cm^{-1} band maxima shift to 3572 cm^{-1} and 3083 cm^{-1} , both of which are consistent with OH- and CH-stretching motions.

The broad feature below 3000 cm^{-1} from the experiments deserves additional attention. Regular signatures in this frequency range were previously reported for thin film liquid PhOH and solid PhOH⁸⁰ and for PhOH at the air/water interface.⁸¹ Such regular structures have been observed also in other hydrogen-bonded systems, such as the acetic acid dimer, and are typically used to characterize a medium-strong hydrogen bond.⁸² They are attributed to a Franck-Condon-like progression of the hydrogen-bond vibration (with a frequency of ca. 50 cm^{-1} in the present case) that is anharmonically coupled to the high-frequency OH stretch vibration.

Simulations for F-PhOH in solution with PC/TIP3P, MTP/TIP3P, and full QM show an extended spectroscopic response in this frequency range with pronounced peaks superimposed which are washed out in the ML/TIP3P simulation and entirely absent in the QM/MM simulations. This suggests that the spectroscopic signature below 3000 cm^{-1} is due to coupling between the H-bonding motion of water around the -COH part of F-PhOH which is primarily sensitive to the nonbonded interactions. To assess whether or not flexibility of the water solvent also affects the spectral signatures, simulations with the reparametrized,^{83,84} flexible KKY (Kumagai, Kawamura, Yokokawa) model were carried out.⁸⁵ One 5 ns simulation with a time step of $\Delta t = 0.25\text{ fs}$ for F-PhOH was run and analyzed. The power spectrum of the F-PhOH OH-stretch vibration confirms the pronounced, regular pattern with peaks separated by some $\sim 50\text{ cm}^{-1}$ below 3000 cm^{-1} , see Figure S2. In addition, the main peak between 3300 cm^{-1} and 3600 cm^{-1} shifts to the red by 78 cm^{-1} compared with simulations

using the rigid TIP3P water model. This confirms that the pattern below 3000 cm^{-1} is due to anharmonic coupling through nonbonded interactions between solute and solvent and not caused by the water internal modes.

For assessing solvent-induced frequency shifts, the frequency distributions from 5 ns simulation of hydrated F-PhOH, analyzed with instantaneous normal modes (INM) for the PC and MTP model are compared with the normal modes from gas phase simulations, see Figures 3 and/or Table S4 for the frequency maxima. For obtaining the instantaneous normal modes the water environment was frozen and the structure of the solute was optimized, followed by a normal mode calculation. The band positions compare well with the frequencies from Table 1. However, the bimodal distribution around 1250 cm^{-1} for both, simulations with PC and MTP, can not be convincingly correlated with the experimental spectra.

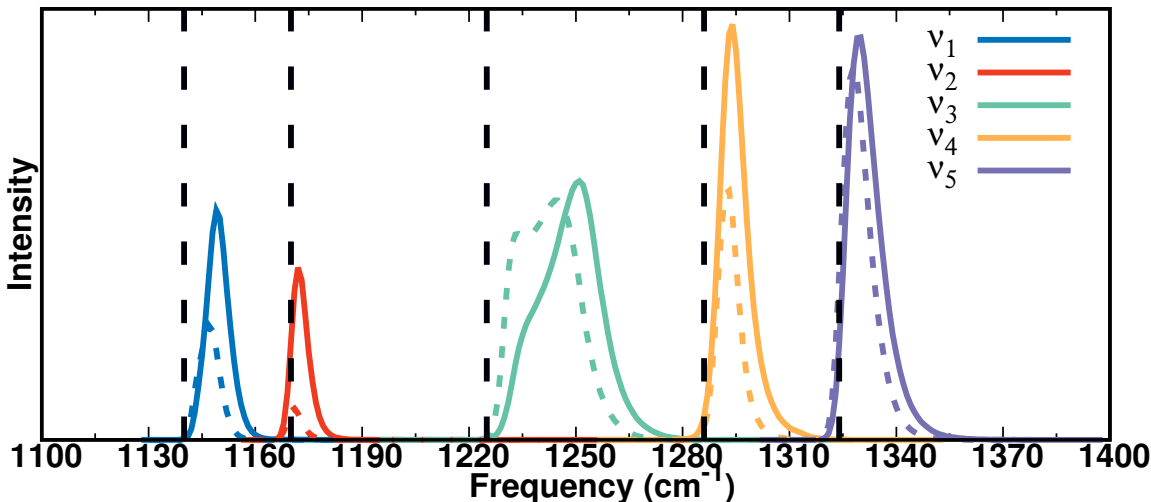


Figure 3: Instantaneous vibrational frequency distributions from 5 ns MTP (solid colored line) and PC (dashed colored line) simulations of F-PhOH in water for five modes between 1100 and 1400 cm^{-1} . The black dashed lines are the harmonic frequencies for the optimized structure in the gas phase using the PC model.

The participation ratios (see Methods) from the MTP simulations of the local modes to the frequencies of the five modes in the $1100\text{ to }1400\text{ cm}^{-1}$ range (ν_1 to ν_5) are shown in

Figure S3. These were determined from the normal modes of F-PhOH over 10^5 snapshots in solution. The contributions of the CF, CO, and CH stretch and the COH bending modes to each of the vibrations between 1100 and 1400 cm^{-1} were determined by projection and the results confirm mixing of these modes.

In summary, the simulations confirm that the modes in the 1100 to 1400 cm^{-1} frequency range in F-PhOH are strongly coupled. Assignment of individual spectral features from comparing experiment with simulations is not obvious. Consistent with experiment the force field-based simulations for the high-frequency modes find a high-frequency ($> 3600\text{ cm}^{-1}$) phenolic -OH stretch together with broad features below 3000 cm^{-1} . These extended absorptions are also found from QM MD simulations without, however, the high-frequency -OH stretch.

Comparison of the Spectroscopy for Hydrated PhOH and F-PhOH

The experimental spectra for F-PhOH (black) and PhOH (green) in water are reported in Figure 2A. For the experimental spectra between 1100 cm^{-1} and 1400 cm^{-1} pronounced differences between the two compounds are found. Most prominently, the single band with maximum at 1242 cm^{-1} for PhOH, which is one of the “X-sensitive modes” involving considerable motion of the phenol ring and the CO group,⁸⁰ is shifted to the red for F-PhOH and split into at least two (at 1201 and 1222 cm^{-1}), but possibly several more peaks, some of which overlap with the peak from PhOH. Other features, such as the broader band with peak maximum at 1381 cm^{-1} for PhOH are also shifted to the red (band maximum at 1368 cm^{-1}) for F-PhOH, see Figure 2A.

Consistent with experiment, the number of spectral features for F-PhOH is larger than for PhOH in the 1200 to 1300 cm^{-1} range. However, none of the computed spectra display

the pronounced double-peak structure above 1200 cm^{-1} for F-PhOH with the broad peak for PhOH to the blue of it. The simulations using MTPs find a single absorption between the low- and high-frequency absorption in F-PhOH, see Figure 2B (green). Considering the CO-power spectrum the feature at 1224 cm^{-1} involves the CO-stretch vibration together with a band at 1283 cm^{-1} . The QM/MM simulations report a larger number of spectroscopic features for PhOH (Figure 2D, green) than experiment does. In particular, the single absorption at 1242 cm^{-1} is not present but rather a broad absorption extending from 1150 up to $\sim 1250\text{ cm}^{-1}$ is found. Finally, simulations using the PhysNet energy function quite well capture the absorption for PhOH at 1270 cm^{-1} (Figure 2E, green) with an additional peak above 1300 cm^{-1} not present in the experiment. Correcting the position 1270 cm^{-1} by 0.94 as was done for the CH- and OH-stretch vibrations shifts this band too far to the red compared with experiment, probably because for coupled vibration the standard correction factor is inappropriate. The absorption for F-PhOH is shifted to the red, in agreement with experiment but does not exhibit the double peak structure. Finally, it should be noted that the experiments are carried out at solute concentrations that favour F-PhOH and PhOH dimers and oligomers to be formed which can affect both, the position of the absorption frequency and the line shape and make direct comparison with simulations potentially difficult.

For the high-frequency part (Figure 2A right panel) the spectra of solvated PhOH and F-PhOH follow each other closely except for a pronounced absorption at 3596 cm^{-1} in PhOH which blue-shifts to 3643 cm^{-1} upon fluorination. This suggests that either electronic coupling between the CF- and OH-sites leads to a slightly stronger OH-bond strength in F-PhOH compared with PhOH, or that the hydration structure around -OH is affected by fluorination, or a combination of the two. From normal mode calculations (MP2/6-31G(d,p)) the OH-stretch vibrations are at 3833 cm^{-1} and 3829 cm^{-1} for PhOH and F-PhOH, which is an insignificant difference and suggests that an electronic origin for the shift is unlikely. For the MTP (3636 and 3588 cm^{-1}) and ML/MM (3794 and 3793 cm^{-1}) simulations the

-OH stretch for PhOH and F-PhOH reproduce the proximity of the two absorptions in solution, but in reverse order compared with experiment. The QM/MM simulations for PhOH (green trace Figure 2D) report the OH-stretch at 3247 cm^{-1} which is to the red of that for F-PhOH (3257 cm^{-1} , orange trace), in agreement with experiment. However, the absorptions are shifted by about 300 cm^{-1} to the red relative to the experimental line positions.

Radial Distribution Functions and Solvent Distribution

Radial distribution functions provide information about solvent-solute interactions. For the F-O_{WAT} and F-H_{WAT} distances they are reported in Figure 4 for the PC, MTP, and ML/MM MD simulations (panels A and B) and for the QM/MM and QM simulations in panels C and D. For $g_{\text{F-O}_\text{W}}$ the position of the first maximum agrees quite favourably for all methods except for simulations with PCs for which the maximum is shifted to shorter separations and the first peak is unusually sharp. Qualitatively, the four other methods find comparable shapes although the two QM simulations have a more pronounced first minimum than MTP and ML/MM simulations which may be related to a somewhat stronger interaction between the fluorine and the water-oxygens or to the shorter sampling time.

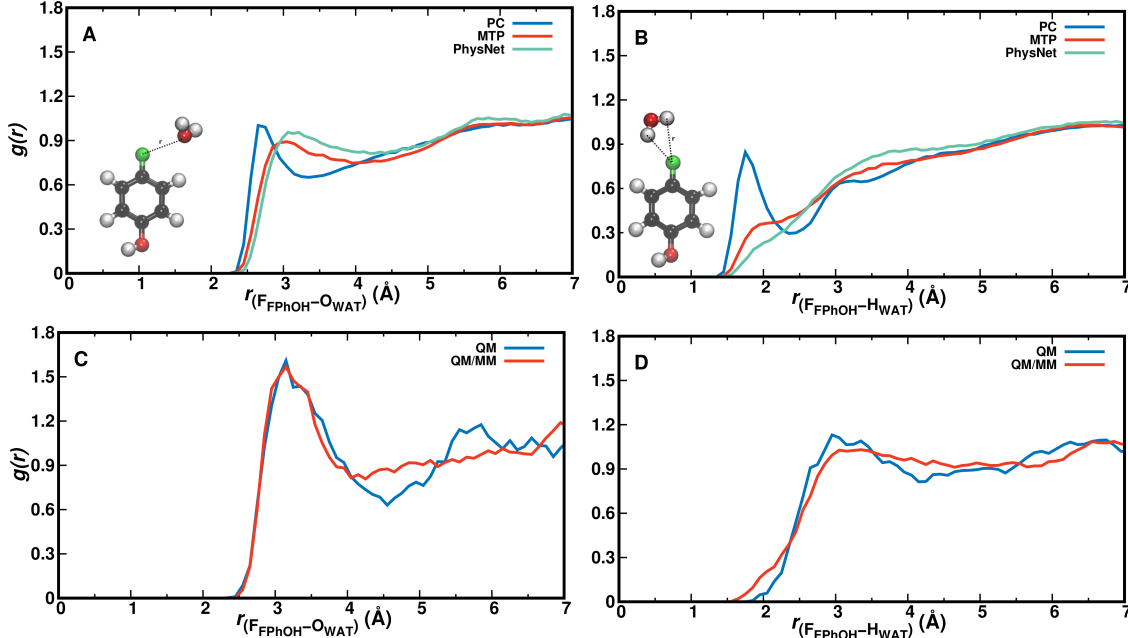


Figure 4: The $g(r)$ for A) F-O_{WAT} and B) F-H_{WAT} separations from PC (blue), MTP (red) and PhysNet (green) simulations of F-PhOH in H₂O. Using PCs both $g(r)$ are more structured whereas the radial distribution functions from MTP and PhysNet - which contains conformationally fluctuating charges - are rather similar to one another. Both, MTP and PhysNet, point to weak interaction between the fluorinated end and the environment. Panels C and D show similar. The scaling along all x -axes is identical whereas that along the y -axis is not.

The F-H_{WAT} pair correlation function g_{F-H_W} shows even more pronounced differences between simulations with PCs compared with all other models. The peak at 1.75 Å points towards a strong, favourable interaction between solvent hydrogen atoms and the fluorine atom which is not found in any of the other four methods. This can be explained by the negative partial charge $q_F = -0.29e$ on the Fluorine atom in the PC model. The MTP and ML/MM simulations find comparable distribution functions whereas the two QM-based simulations differ from this in that the broad first maximum is peaked at around 3 Å with the full QM simulations and shows a more pronounced local minimum. All distribution functions except that with PCs report the first maximum at an F-O_W separation of ~ 3 Å which points towards a largely hydrophobic behaviour of the CF site. This is also consistent with notions from pharmaceutical chemistry in that a CF group reduces ligand solvation and

increases its hydrophobicity.²⁷ The number of water molecules within distance r is reported in Figure S4 and shows that for small F–water separations ($r \leq 4$ Å) the occupation from simulations with MTP and PhysNet is similar but clearly below that of QM/MM and QM simulations (which are identical) whereas for larger separations ($r \sim 5$ Å) that from QM simulations approaches the MTP and PhysNet simulations.

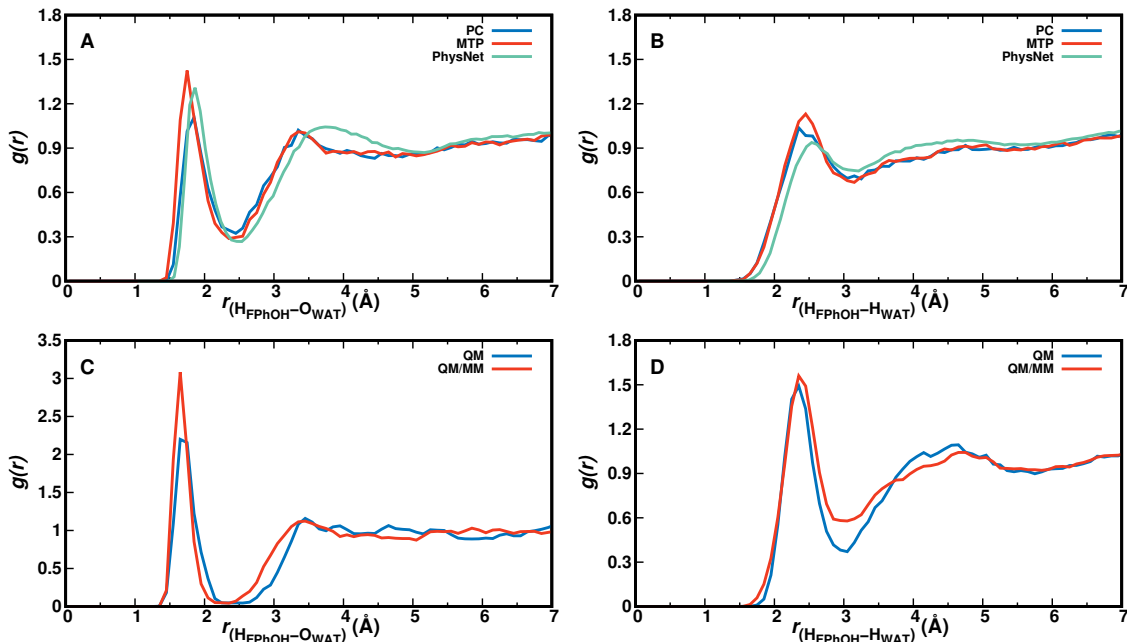


Figure 5: The $g(r)$ for A) $\text{H}_{\text{FPhOH}}/\text{PhOH}-\text{O}_{\text{WAT}}$ and B) $\text{H}_{\text{FPhOH}}/\text{PhOH}-\text{H}_{\text{WAT}}$ distances between the H-atom of the solute OH-group as obtained from PC (blue), MTP (red) and PhysNet (green) simulations for F-PhOH in H_2O . Panels C and D from QM and QM/MM simulations. The scaling along all x -axes is identical whereas that along the y -axis it is not.

For analyzing hydration around the hydroxyl group the $\text{H}_{\text{OH}}-\text{O}_{\text{WAT}}$ and $\text{H}_{\text{OH}}-\text{H}_{\text{WAT}}$ pair correlation functions were considered, see Figure 5. From simulations using the PC, MTP, and PhysNet models $g_{\text{H}_{\text{OH}}-\text{O}_{\text{W}}}$ characterizing the hydrogen bond between OH and water-oxygen atoms is similar up to and including the first minimum, see Figure 5A. The second maximum shifts to somewhat larger separations for the PhysNet simulations. Similar observations are made for $g_{\text{H}_{\text{OH}}-\text{H}_{\text{W}}}$ in panel B. The hydrogen-bond pair distribution function with a first maximum at ~ 1.6 Å suggests that solvent water molecules are quite strongly bound to the

-OH group and that the solvent water at the -OH group exchanges.

For $g_{\text{H}_{\text{OH}}-\text{O}_{\text{W}}}$ from the QM and QM/MM simulations (blue and red traces in Figure 5C) the position of the first maximum is almost identical whereas the height of the first peak differs. Both pair correlation functions have a first minimum around 2.5 Å with an amplitude close to 0 which suggests that during the 25 ps simulation one solvent water molecule is strongly bound to the OH-group of F-PhOH and does not exchange with the surrounding solvent. As a consequence the “free phenolic -OH stretch” (spectroscopic feature around and above 3600 cm^{-1} , Figure 2) is absent in the QM MD simulations, in contrast with what was found from the experiments and from the PC, MTP, and ML/MM MD simulations. On the other hand, the radial distribution function between the water-oxygen atoms and the two carbon atoms flanking the COH group in F-PhOH from a 5 ns MTP simulation (Figure S5) demonstrates that the solvent distribution dynamics is exhaustively sampled on the 5 ns time scale.

For the phenolic oxygen as an H-bond acceptor the $\text{O}-\text{H}_{\text{WAT}}$ and $\text{O}-\text{O}_{\text{WAT}}$ pair correlation functions for F-PhOH are reported in Figure S6. Panels A and B provide a direct comparison of the three force field-based simulations whereas panels C and D are those from the QM and QM/MM simulations, respectively. The MTP simulations (red) find strongest localization of the water followed by PC (blue) and PhysNet (green) simulations. For the QM simulations the first minimum for $g_{\text{O}-\text{O}_{\text{W}}}$ is deeper than for the QM-MM simulations whereas the position and height of the first maximum are comparable. The radial distribution functions from simulations with MTP are closest to those from the QM and QM/MM simulations, respectively.

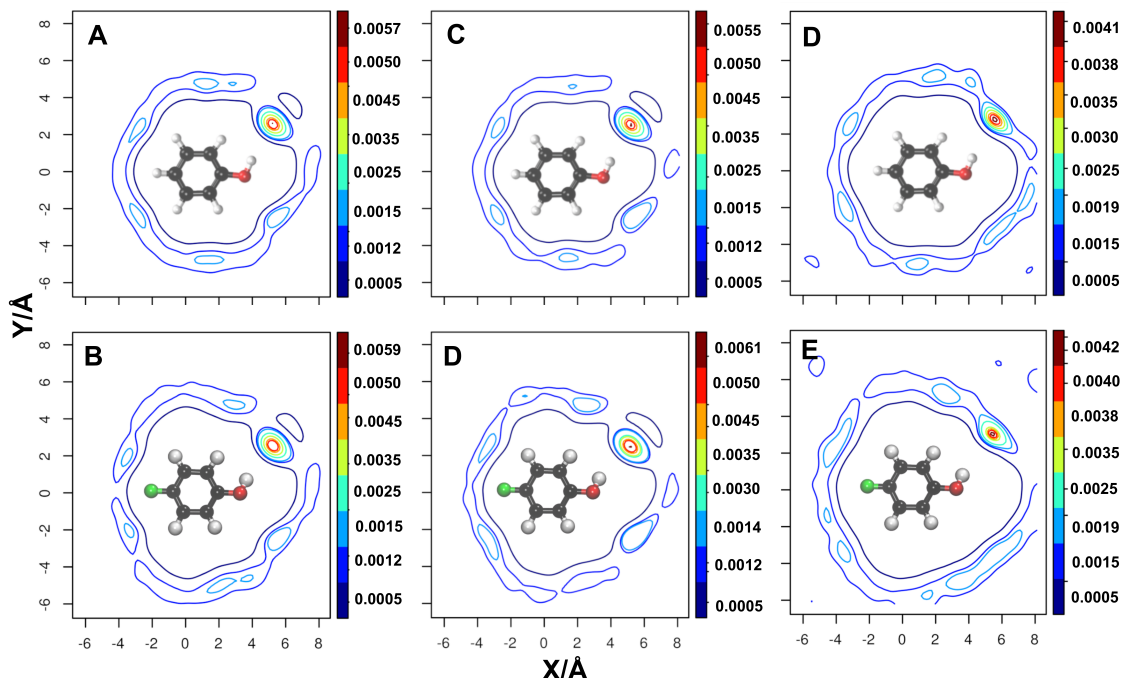


Figure 6: 2-dimensional solvent distribution from reorienting snapshots with respect to all heavy atoms of the solute, including the phenolic oxygen atom. Solvent distributions around PhOH and F-PhOH for PC (panel A and B), MTP (panel C and D) and from PhysNet (panel E and F) model. The iso-contour values are shown in each panel. For the solvent distribution upon reorienting with respect to all heavy atoms excluding the phenolic oxygen atom, see Figure S7 which manifestly shows symmetric water distribution according to the underlying dynamically averaged spatial symmetry of the solute due to rotation of the OH group around the -COH axis, see Figure S8.

Two-dimensional solvent distribution functions were generated from the positions of the water-oxygen atoms around F-PhOH. For that, the structures of the 5000 snapshots were oriented with C1 in the origin, the C1–C4 bond along the x -axis the [C1,C4,H] atoms in the xy -plane. A 2-dimensional histogram of the water positions was generated and then refined from kernel density estimation using Rstudio.⁸⁶ The distribution of the solvent water around the CF-part of F-PhOH is comparatively flat for all simulations with PC, MTP and PhysNet when contrasted with the COH-moiety of the solute, see Figure 6. It is also found that for PhOH (top line) the solvent distributions resemble those for F-PhOH (bottom line). The asymmetry in the solvent distribution around the -COH group is due to the reference atoms chosen for the superposition of all structures. If the phenol-oxygen atom is excluded in

reorienting the structures the 2d distribution becomes manifestly symmetric (Figure S7) and also clarifies that the -OH group of the solute rotates on the time scale of the simulations, see Figure S8. Specifically, rotation of the -COH group is an activated process and occurs on the ~ 100 ps time scale from MTP and ML/MM simulations.

The weak interaction between solvent and solute around the CF-site of F-PhOH can also be gleaned from the behaviour of the frequency fluctuation correlation functions (FFCFs). For this, the FFCFs were determined from the frequency trajectories $\omega_i(t)$ for the five modes in the CF-stretch region, i.e. ν_1 to ν_5 , between 1100 cm^{-1} and 1400 cm^{-1} and for the OH-stretch vibration, see Figures S9 and S10. The FFCFs contain information about the coupling between a particular mode and the environmental dynamics. The fitting parameters for ν_1 to ν_5 in Table S5 show that the fast correlation is generally $\tau_1 \sim 0.1$ ps whereas the longer time scale ranges from $\tau_2 = 0.28$ ps to $\tau_2 = 0.83$ ps. Such short correlation times point towards weak solvent/solute interactions close to the CF-site. The static components Δ_0 are very small, too, which also imply rapid, unspecific dynamics around the CF-group. For the OH-stretch vibration, the fast correlation time is $\tau_1 \sim 0.1$ ps while the longer one is $\tau_1 \sim 0.5$ ps which are comparatively short. Compared with the FFCFs for vibrations involving the CF-stretch the $t = 0$ amplitude and the static offset Δ_0 is larger by one to two orders of magnitude which points towards somewhat slower dynamics around the OH bond of F-PhOH.

Discussion and Conclusion

The present work discusses the infrared spectroscopy of and solvent distribution around F-PhOH in water from experiments and a range of computational approaches including full QM, QM/MM, PC-based, MTP-based and ML/MM simulations. The simulations show that

the modes in the range between 1200 and 1300 cm^{-1} are heavily mixed which complicates the assignment of the spectroscopic features. Accounting for the known overestimation of frequencies from MP2/6-31G(d,p) calculations the ML/MM simulations best capture the experimentally observed patterns in this frequency range. The solute-solvent pair distribution functions together with the FFCFs indicate that interaction between the fluorinated position and the environment is weak as has also been found earlier for fluoro-acetonitrile.⁴⁹

For the phenol-OH-stretch vibration both, “gas phase” (around 3600 cm^{-1}) and “water-phenol hydrogen bonded” signatures (below 3000 cm^{-1}) are found from experiments and the simulations. A regular pattern with a spacing of $\sim 50 \text{ cm}^{-1}$ is reminiscent of recent SFG spectra of PhOH at the air/water interface and earlier experiments on liquid and solid pure PhOH⁸⁰ and is assigned to water-phenol hydrogen bonded motions. For the high frequency (OH-stretch) modes early experiments for PhOH vapor, in apolar solvent (CCl_4) and as a liquid reported band positions at $\sim 3650 \text{ cm}^{-1}$, $\sim 3600 \text{ cm}^{-1}$, and at 3500 cm^{-1} , respectively.⁸⁰ In CCl_4 solution and the pure liquid an additional band is at 3350 cm^{-1} .⁸⁰ The present work finds a sharp peak at 3596 cm^{-1} which is assigned to the “free” phenol-OH stretch in a non-hydrogen bonded environment. This is supported by the observation that the peak is only marginally shifted from the PhOH OH-stretch in vapor and the fact that the spectroscopic feature is sharp and therefore can not be due to water.

More recently, infrared spectra were recorded for PhOH complexed with variable numbers of water molecules in the gas phase,^{87,88} in matrices,⁸⁹ and for PhOH at the air/water interface using vibrational sum frequency generation (SFG).⁸¹ The cluster studies all report the phenolic-OH stretch vibration at frequencies above 3000 cm^{-1} whereas the experiment at the air/water interface assigns a very broad signature in the SFG signal extending from 2550 cm^{-1} to 3500 cm^{-1} to the OH-stretch mode.⁸¹ This finding is consistent with the present experiments which report a broad absorption for both, F-PhOH and PhOH extending down

to $\sim 2700\text{ cm}^{-1}$ which is also assigned to the phenol-OH stretch for water-coordinated -COH, see Figures 2 and S2.

Hydration around the -CF group as characterized by 1d- and 2d-solvent distribution functions does not feature any pronounced hydrogen bonding unless a conventional PC model is used which, however, exaggerates the directed interaction along the CF bond. On the other hand, solvent water molecules form intermittent H-bonds with the -OH group of F-PhOH which leads to the broad spectroscopic response below 3000 cm^{-1} observed experimentally and reproduced by several of the computational models.

From the perspective of halogenic modifications of organic frameworks used for drug design the present work suggests that the local hydration of -CH and -CF groups is comparable (see Figures 4 and S5), supporting the notion that “F behaves like a large H-atom”.²⁷ Although the C-F bond has three isolated electron pairs, it has weaker electrostatic interactions compared to O due to the small size and high electronegativity, which compromises its hydrogen bonding ability and can thus better be described as a weakly polar interaction rather than a hydrogen bond. Such insights are important guidelines for rational drug discovery as they provide a basis for directed modification and evolution of ligands with specific interactions in protein binding sites.

Supporting Information Available

The supporting information provides tables for the force field parametrizations (Tables S1 to S3), frequency maxima for frequency distributions (Table S4), and parameters for the FFCEs (Table S5) together with Figures S1 to S10 the report quality of the PhysNet model, additional solvent distribution functions, dihedral time series and the FFCEs for the CF-

and OH-stretch frequencies.

Acknowledgments

This work was supported by the Swiss National Science Foundation, NCCR MUST (to MM, PH and UR).

References

- (1) Herrera-Rodriguez, L.; Khan, F.; Robins, K.; Meyer, H.-P. Perspectives on biotechnological halogenation. Part I: Halogenated products and enzymatic halogenation. *Chim. Oggi* **2011**, *29*, 31–33.
- (2) Hernandez, M. Z.; Cavalcanti, S. M. T.; Moreira, D. R. M.; de Azevedo, J.; Filgueira, W.; Leite, A. C. L. Halogen atoms in the modern medicinal chemistry: hints for the drug design. *Curr. Drug Targets* **2010**, *11*, 303–314.
- (3) Matter, H.; Nazar, M.; Gssregen, S.; Will, D.; Schreuder, H.; Bauer, A.; Urmann, M.; Ritter, K.; Wagner, M.; Wehner, V. Evidence for C–Cl/C–Br $\cdots\pi$ Interactions as an Important Contribution to ProteinLigand Binding Affinity. *Angew. Chem. Int. Ed.* **2009**, *48*, 2911–2916.
- (4) Müller, K.; Faeh, C.; Diederich, F. Fluorine in Pharmaceuticals: Looking Beyond Intuition. *Science* **2007**, *317*, 1881–1886.
- (5) Metrangolo, P.; Neukirch, H.; Pilati, T.; Resnati, G. Halogen Bonding Based Recognition Processes: A World Parallel to Hydrogen Bonding. *Acc. Chem. Res.* **2005**, *38*, 386–395.

- (6) Metrangolo, P.; Meyer, F.; Pilati, T.; Resnati, G.; Terraneo, G. Halogen Bonding in Supramolecular Chemistry. *Angew. Chem. Int. Ed.* **2008**, *47*, 6114–6127.
- (7) Lommerse, J. P. M.; Stone, A. J.; Taylor, R.; Allen, F. H. The Nature and Geometry of Intermolecular Interactions between Halogens and Oxygen or Nitrogen. *J. Am. Chem. Soc.* **1996**, *118*, 3108–3116.
- (8) Auffinger, P.; Hays, F. A.; Westhof, E.; Ho, P. S. Halogen bonds in biological molecules. *Proc. Natl. Acad. Sci.* **2004**, *101*, 16789–16794.
- (9) Riley, K. E.; Hobza, P. Strength and Character of Halogen Bonds in ProteinLigand Complexes. *Cryst. Growth Des.* **2011**, *11*, 4272–4278.
- (10) Hardegger, L. A.; Kuhn, B.; Spinnler, B.; Anselm, L.; Ecabert, R.; Stihle, M.; Gsell, B.; Thoma, R.; Diez, J.; Benz, J. et al. Systematic Investigation of Halogen Bonding in ProteinLigand Interactions. *Angew. Chem. Int. Ed.* **2011**, *50*, 314–318.
- (11) Riley, K.; Murray, J.; Fanfrlík, J.; Řezáč, J.; Solá, R.; Concha, M.; Ramos, F.; Politzer, P. Halogen bond tunability I: the effects of aromatic fluorine substitution on the strengths of halogen-bonding interactions involving chlorine, bromine, and iodine. *J. Mol. Model.* **2011**, *17*, 3309–3318.
- (12) El Hage, K.; Piquemal, J.-P.; Hobaika, Z.; Maroun, R. G.; Gresh, N. Could the “Janus-like” properties of the halobenzene CX bond (X=Cl, Br) be leveraged to enhance molecular recognition? *J. Comp. Chem.* **2015**, *36*, 210–221.
- (13) Lu, Y.; Shi, T.; Wang, Y.; Yang, H.; Yan, X.; Luo, X.; Jiang, H.; Zhu, W. Halogen BondingA Novel Interaction for Rational Drug Design? *J. Med. Chem.* **2009**, *52*, 2854–2862.
- (14) Wilcken, R.; Zimmermann, M. O.; Lange, A.; Joerger, A. C.; Boeckler, F. M. Principles

- and Applications of Halogen Bonding in Medicinal Chemistry and Chemical Biology. *J. Med. Chem.* **2013**, *56*, 1363–1388.
- (15) El Hage, K.; Pandeyarajan, V.; Phillips, N. B.; Smith, B. J.; Menting, J. G.; Whittaker, J.; Lawrence, M. C.; Meuwly, M.; Weiss, M. A. Extending halogen-based medicinal chemistry to proteins. *J. Biol. Chem.* **2016**, *291*, 27023–27041.
- (16) Desiraju, G. R.; Ho, P. S.; Kloo, L.; Legon, A. C.; Marquardt, R.; Metrangolo, P.; Politzer, P.; Resnati, G.; Rissanen, K. Definition of the halogen bond (IUPAC Recommendations 2013). *Pure Appl. Chem.* **2013**, *85*, 1711–1713.
- (17) Clark, T.; Hennemann, M.; Murray, J. S.; Politzer, P. Halogen bonding: the sigma-hole. *J. Mol. Model.* **2007**, *13*, 291–296.
- (18) Wang, H.; Wang, W.; Jin, W. J. sigma-Hole Bond vs pi-Hole Bond: A Comparison Based on Halogen Bond. *Chem. Rev.* **2016**, *116*, 5072–5104.
- (19) Neaton, J. B. CHEMISTRY A direct look at halogen bonds. *Science* **2017**, *358*, 167–168.
- (20) Kawai, S.; Sadeghi, A.; Xu, F.; Peng, L.; Orita, A.; Otera, J.; Goedecker, S.; Meyer, E. Extended Halogen Bonding between Fully Fluorinated Aromatic Molecules. *ACS NANO* **2015**, *9*, 2574–2583.
- (21) Metrangolo, P.; Murray, J. S.; Pilati, T.; Politzer, P.; Resnati, G.; Terraneo, G. The fluorine atom as a halogen bond donor, viz. a positive site. *CrystEngComm* **2011**, *13*, 6593–6596.
- (22) Politzer, P.; Murray, J. S.; Clark, T. Halogen bonding and other sigma-hole interactions: a perspective. *Phys. Chem. Chem. Phys.* **2013**, *15*, 11178–11189.
- (23) Legon, A. Prereactive complexes of dihalogens XY with Lewis bases B in the gas phase:

- A systematic case for the halogen analogue B–XY of the hydrogen bond B–HX. *Angew. Chem., Int. Ed.* **1999**, *38*, 2687–2714.
- (24) Shah, P.; Westwell, A. D. The role of fluorine in medicinal chemistry. **2007**, *22*, 527–540.
- (25) Barbarich, T.; Rithner, C.; Miller, S.; Anderson, O.; Strauss, S. Significant inter- and intramolecular O–H center dot center dot center dot FC hydrogen bonding. *J. Am. Chem. Soc.* **1999**, *121*, 4280–4281.
- (26) Chopra, D.; Row, T. N. G. Role of organic fluorine in crystal engineering. *CrystEngComm* **2011**, *13*, 2175–2186.
- (27) Hevey, R. The Role of Fluorine in Glycomimetic Drug Design. *Chem. Eur. J* **2021**, *27*, 2240–2253.
- (28) OHagan, D.; S. Rzepa, H. Some influences of fluorine in bioorganic chemistry. *Chem. Commun.* **1997**, 645–652.
- (29) Brooks, B. R.; Brooks III, C. L.; MacKerell Jr., A. D.; Nilsson, L.; Petrella, R. J.; Roux, B.; Won, Y.; Archontis, G.; Bartels, C.; Boresch, S. et al. CHARMM: The Biomolecular Simulation Program. *J. Comp. Chem.* **2009**, *30*, 1545–1614.
- (30) Vanommeslaeghe, k.; hatcher, E.; Acharya, C.; Kundu, S.; Zhong, S.; Shim, J.; Darian, E.; Guvench, O.; Lopes, P.; Vorobyov, I. et al. CHARMM general force field: A force field for drug-like molecules compatible with the CHARMM all-atom additive biological force fields. *J. Comp. Chem.* **2010**, *31*, 671–690.
- (31) Kramer, C.; Gedeck, P.; Meuwly, M. Atomic Multipoles: Electrostatic Potential Fit, Local Reference Axis Systems and Conformational Dependence. *J. Comp. Chem.* **2012**, *33*, 1673–1688.

- (32) Bereau, T.; Kramer, C.; Meuwly, M. Leveraging Symmetries of Static Atomic Multipole Electrostatics in Molecular Dynamics Simulations. *J. Chem. Theo. Comp.* **2013**, *9*, 5450–5459.
- (33) El Hage, K.; Bereau, T.; Jakobsen, S.; Meuwly, M. Impact of Quadrupolar Electrostatics on Atoms Adjacent to the Sigma-Hole in Condensed-Phase Simulations. *J. Chem. Theo. Comp.* **2016**, *12*, 3008–3019.
- (34) El Hage, K.; Gupta, P. K.; Bemish, R.; Meuwly, M. Molecular Mechanisms Underlying Solute Retention at Heterogeneous Interfaces. *J. Phys. Chem. Lett.* **2017**, *8*, 4600–4607.
- (35) Hedin, F.; El Hage, K.; Meuwly, M. A Toolkit to Fit Nonbonded Parameters from and for Condensed Phase Simulations. *J. Chem. Theo. Comp.* **2016**, *56*, 1479–1489.
- (36) Jorgensen, W. L.; Chandrasekhar, J.; Madura, J. D.; Impey, R. W.; Klein, M. L. Comparison of Simple Potential Functions for Simulating Liquid Water. *J. Chem. Phys.* **1983**, *79*, 926–935.
- (37) Swope, W. C.; Andersen, H. C.; Berens, P. H.; Wilson, K. R. A Computer Simulation Method for the Calculation of Equilibrium Constants for the Formation of Physical Clusters of Molecules: Application to Small Water Clusters. *J. Chem. Phys.* **1982**, *76*, 637–649.
- (38) Steinbach, P. J.; Brooks, B. R. New Spherical-Cutoff Methods for Long-Range Forces in Macromolecular Simulation. *J. Comp. Chem.* **1994**, *15*, 667–683.
- (39) Darden, T.; York, D.; Pedersen, L. Particle Mesh Ewald: An Nlog(N) Method for Ewald Sums in Large Systems. *J. Chem. Phys.* **1993**, *98*, 10089–10092.
- (40) Ryckaert, J.-P.; Ciccotti, G.; Berendsen, H. J. C. Numerical integration of the cartesian equations of motion of a system with constraints: molecular dynamics of n-alkanes. *J. Comp. Phys.* **1977**, *23*, 327–341.

- (41) Gunsteren, W. V.; Berendsen, H. Algorithms for Macromolecular Dynamics and Constraint Dynamics. *Mol. Phys.* **1997**, *34*, 1311–1327.
- (42) Larsen, A. H.; Mortensen, J. J.; Blomqvist, J.; Castelli, I. E.; Christensen, R.; Duřak, M.; Friis, J.; Groves, M. N.; Hammer, B.; Hargus, C. et al. The atomic simulation environment – a Python library for working with atoms. *J. Phys. Condens. Matter* **2017**, *29*, 273002.
- (43) Spohr, E. Effect of electrostatic boundary conditions and system size on the interfacial properties of water and aqueous solutions. *J. Chem. Phys.* **1997**, *107*, 6342–6348.
- (44) Loncharich, R. J.; Brooks, B. R.; Pastor, R. W. Langevin dynamics of peptides: The frictional dependence of isomerization rates of N-acetylalanyl-N-methylamide. *Biopolymers* **1992**, *32*, 523–535.
- (45) Thomas, M.; Brehm, M.; Fligg, R.; Vhringer, P.; Kirchner, B. Computing vibrational spectra from ab initio molecular dynamics. *Phys. Chem. Chem. Phys.* **2013**, *15*, 6608–6622.
- (46) Schmitz, M.; Tavan, P. Vibrational spectra from atomic fluctuations in dynamics simulations. I. Theory, limitations, and a sample application. *J. Chem. Phys.* **2004**, *121*, 12233–12246.
- (47) Schmitz, M.; Tavan, P. Vibrational spectra from atomic fluctuations in dynamics simulations. II. Solvent-induced frequency fluctuations at femtosecond time resolution. *J. Chem. Phys.* **2004**, *121*, 12247–12258.
- (48) Hamm, P.; Zanni, M. *Concepts and Methods of 2D Infrared Spectroscopy*; Cambridge University Press: New York, 2011.
- (49) Cazade, P.-A.; Tran, H.; Bereau, T.; Das, A. K.; Klaesi, F.; Hamm, P.; Meuwly, M. Sol-

- vation of fluoro-acetonitrile in water by 2D-IR spectroscopy: A combined experimental-computational study. *J. Chem. Phys.* **2015**, *142*.
- (50) Moller, K.; Rey, R.; Hynes, J. Hydrogen Bond Dynamics in Water and Ultrafast Infrared Spectroscopy: A Theoretical Study. *J. Phys. Chem. A* **2004**, *108*, 1275–1289.
- (51) Salehi, M.; Koner, D.; Meuwly, M. Vibrational Spectroscopy of N_3^- in the Gas- and Condensed-Phase. *J. Phys. Chem. B* **2019**, *123*, 3282–3290.
- (52) Virtanen, P.; Gommers, R.; Oliphant, T. E.; Haberland, M.; Reddy, T.; Cournapeau, D.; Burovski, E.; Peterson, P.; Weckesser, W.; Bright, J. et al. SciPy 1.0: Fundamental Algorithms for Scientific Computing in Python. *Nature Methods* **2020**, *17*, 261–272.
- (53) Car, R.; Parrinello, M. Unified Approach for Molecular Dynamics and Density-Functional Theory. *Phys. Rev. Lett.* **1985**, *55*, 2471–2474.
- (54) CPMD, Copyright IBM Corp 1990-2019, Copyright MPI für Festkörperforschung Stuttgart 1997-2001. <http://www.cpmc.org/>, <http://www.cpmc.org/>.
- (55) Becke, A. D. Density-functional exchange-energy approximation with correct asymptotic behavior. *Phys. Rev. A* **1988**, *38*, 3098.
- (56) Lee, C.; Yang, W.; Parr, R. G. Development of the Colle-Salvetti correlation-energy formula into a functional of the electron density. *Phys. Rev. B* **1988**, *37*, 785–789.
- (57) von Lilienfeld, O. A.; Tavernelli, I.; Rothlisberger, U.; Sebastiani, D. Optimization of Effective Atom Centered Potentials for London Dispersion Forces in Density Functional Theory. *Phys. Rev. Lett.* **2004**, *93*, 153004.
- (58) Lin, I.-C.; Coutinho-Neto, M. D.; Felsenheimer, C.; von Lilienfeld, O. A.; Tavernelli, I.; Rothlisberger, U. Library of dispersion-corrected atom-centered potentials for general-

- ized gradient approximation functionals: Elements H, C, N, O, He, Ne, Ar, and Kr. *Phys. Rev. B* **2007**, *75*, 205131.
- (59) Doemer, M.; Tavernelli, I.; Rothlisberger, U. Intricacies of Describing Weak Interactions Involving Halogen Atoms within Density Functional Theory. *J. Chem. Theory Comput.* **2013**, *9*, 955–964, PMID: 26588739.
- (60) Troullier, N.; Martins, J. L. Efficient pseudopotentials for plane-wave calculations. *Phys. Rev. B* **1991**, *43*, 1993.
- (61) Zierkiewicz, W.; Michalska, D. Molecular Structure and Infrared Spectra of 4-Fluorophenol: A Combined Theoretical and Spectroscopic Study. *J. Phys. Chem.* **2003**, *107*, 4547–4554.
- (62) van Gunsteren, W. F.; coworkers, Biomolecular Simulation: The GROMOS96 Manual and User Guide; vdf Hochschulverlag AG an der ETH Zürich and BIOMOS b.v. Groningen: Zürich, Switzerland and The Netherlands, 2006. <http://www.gromos.net/>, <http://www.gromos.net/>.
- (63) Laio, A.; VandeVondele, J.; Rothlisberger, U. A Hamiltonian electrostatic coupling scheme for hybrid CarParrinello molecular dynamics simulations. *J. Chem. Phys.* **2002**, *116*, 6941–6947.
- (64) Colombo, M. C.; Guidoni, L.; Laio, A.; Magistrato, A.; Maurer, P.; Piana, S.; Röhrig, U.; Spiegel, K.; Sulpizi, M.; VandeVondele, J. et al. Hybrid QM/MM CarParrinello Simulations of Catalytic and Enzymatic Reactions. *CHIMIA International Journal for Chemistry* **2002**, *56*, 13–19.
- (65) Brunk, E.; Rothlisberger, U. Mixed Quantum Mechanical/Molecular Mechanical Molecular Dynamics Simulations of Biological Systems in Ground and Electronically Excited States. *Chem. Rev.* **2015**, *115*, 6217–6263.

- (66) Case, D. A.; Ben-Shalom, I. Y.; Brozell, S. R.; Cerutti, D. S.; Cheatham III, T. E.; Cruzeiro, V. W. D.; Darden, T. A.; Duke, R. E.; Ghoreishi, D.; Gilson, M. K. et al. AMBER 2018, University of California, San Francisco. <http://ambermd.org/>, <http://ambermd.org/>.
- (67) Wang, J.; Wolf, R. M.; Caldwell, J. W.; Kollman, P. A.; Case, D. A. Development and testing of a general amber force field. *J. Comput. Chem.* **25**, 1157–1174.
- (68) GAFF2 is a public domain forcefield, an upgrade of the previously released general AMBER forcefield (GAFF). It is available with the distribution of AmberTools17 and can be downloaded from <http://ambermd.org>. A publication for it is currently under preparation. <http://ambermd.org/>, <http://ambermd.org/>.
- (69) Berendsen, H. J. C.; Postma, J. P. M.; van Gunsteren, W. F.; DiNola, A.; Haak, J. R. Molecular dynamics with coupling to an external bath. *J. Chem. Phys.* **1984**, *81*, 3684–3690.
- (70) Unke, O. T.; Meuwly, M. PhysNet: A neural network for predicting energies, forces, dipole moments, and partial charges. *J. Chem. Theo. Comp.* **2019**, *15*, 3678–3693.
- (71) Gilmer, J.; Schoenholz, S. S.; Riley, P. F.; Vinyals, O.; Dahl, G. E. Neural message passing for quantum chemistry. Proc. of the 34th Int. Conf. on Machine Learning-Volume 70. 2017; pp 1263–1272.
- (72) Werner, H.-J.; Knowles, P. J.; Knizia, G.; Manby, F. R.; Schütz, M.; Celani, P.; Györffy, W.; Kats, D.; Korona, T.; Lindh, R. et al. MOLPRO, version 2019, a package of ab initio programs. 2019.
- (73) Smith, J. S.; Isayev, O.; Roitberg, A. E. ANI-1, A data set of 20 million calculated off-equilibrium conformations for organic molecules. *Sci. Data* **2017**, *4*, 170193.

- (74) Michalska, D.; Zierkiewicz, W.; Bienko, D. C.; Wojciechowski, W.; Zeegers-Huyskens, T. Troublesome Vibrations of Aromatic Molecules in Second-Order Moller-Plesset and Density Functional Theory Calculations: Infrared Spectra of Phenol and Phenol-OD. *J. Phys. Chem.* **2001**, *105*, 8734–8739.
- (75) Bist, H.; Brand, J. C.; Williams, D. The vibrational spectrum and torsion of phenol. *J. Mol. Spectrosc.* **1967**, *24*, 402–412.
- (76) Bauer, B.; Reynolds, M. Recovering data from scanned graphs: Performance of Frantz’s g3data software. *Behav. Res. Meth.* **2008**, *40*, 858–868.
- (77) Morino, Y.; Kuchitsu, K. A Note on the Classification of Normal Vibrations of Molecules. *J. Chem. Phys.* **1952**, *20*, 1809–1810.
- (78) Scott, A. P.; Radom, L. Harmonic Vibrational Frequencies: An Evaluation of HartreeFock, MllerPlesset, Quadratic Configuration Interaction, Density Functional Theory, and Semiempirical Scale Factors. *J. Phys. Chem.* **1996**, *100*, 10502–16513.
- (79) Mizuse, K.; Hamashima, T.; Fujii, A. Infrared spectroscopy of phenol-(H₂O) $n > 10$: structural strains in hydrogen bond networks of neutral water clusters. *J. Phys. Chem. A* **2009**, *113*, 12134–12141.
- (80) Evans, J. The vibrational spectra of phenol and phenol-OD. *Spectrochim. Act.* **1960**, *16*, 1382–1392.
- (81) Kusaka, R.; Ishiyama, T.; Nihonyanagi, S.; Morita, A.; Tahara, T. Structure at the air/water interface in the presence of phenol: a study using heterodyne-detected vibrational sum frequency generation and molecular dynamics simulation. *Phys. Chem. Chem. Phys.* **2018**, *20*, 3002–3009.
- (82) Nibbering, E. T.; Dreyer, J.; Kühn, O.; Bredenbeck, J.; Hamm, P.; Elsaesser, T. *Analysis and control of ultrafast photoinduced reactions*; Springer, 2007; pp 619–687.

- (83) Burnham, C. J.; Li, J. C.; Leslie, M. Molecular Dynamics Calculations for Ice Ih. *J. Phys. Chem. B* **1997**, *101*, 6192–6195.
- (84) Plattner, N.; Meuwly, M. Atomistic Simulations of CO Vibrations in Ices Relevant to Astrochemistry. *ChemPhysChem* **2008**, *9*, 1271–1277.
- (85) Kumagai, N.; Kawamura, K.; Yokokawa, T. An Interatomic Potential Model for H₂O: Applications to Water and Ice Polymorphs. *Mol. Sim.* **1994**, *12*, 177–186.
- (86) RStudio Team, RStudio: Integrated Development Environment for R. RStudio, PBC.: Boston, MA, 2020.
- (87) Hamashima, T.; Mizuse, K.; Fujii, A. Spectral Signatures of Four-Coordinated Sites in Water Clusters: Infrared Spectroscopy of Phenol-(H₂O)_n ($20 \leq n \leq 50$). *J. Phys. Chem. A* **2011**, *115*, 620–625.
- (88) Shimamori, T.; Fujii, A. Infrared spectroscopy of warm and neutral phenol–water clusters. *J. Phys. Chem. A* **2015**, *119*, 1315–1322.
- (89) Banerjee, P.; Bhattacharya, I.; Chakraborty, T. Cooperative effect on phenolic ν O–H frequencies in 1: 1 hydrogen bonded complexes of o-fluorophenols with water: A matrix isolation infrared spectroscopic study. *Spectrochim. Act.* **2017**, *181*, 116–121.

Supporting Information: Hydration Dynamics and 1D/2D Spectroscopy of 4-Fluorophenol

Seyedeh Maryam Salehi, Silvan Käser, Kai Töpfer,[†] Polydefkis Diamantis,[‡]

Peter Hamm,[¶] Ursula Rothlisberger,[‡] and Markus Meuwly^{*,†}

[†]*Department of Chemistry, University of Basel, Klingelbergstrasse 80 , CH-4056 Basel,
Switzerland.*

[‡]*Laboratory of Computational Chemistry and Biochemistry, Institute of Chemical Sciences
and Engineering, École Polytechnique Fédérale de Lausanne, CH-1015 Lausanne,
Switzerland.*

[¶]*Department of Chemistry, University of Zurich*

E-mail: m.meuwly@unibas.ch

Table S1: Molecular monopoles calculated using a fitting environment with GDMA algorithm for PhOH and F-PhOH.¹

Atom (PhOH)	Charge (e)	Atom (F-PhOH)	charge (e)
C1	-0.095	C1	0.161
C2	-0.074	C2	-0.060
C3	-0.079	C3	-0.061
C4	0.075	C4	0.064
C5	-0.079	C5	-0.061
C6	-0.074	C6	-0.060
H7	0.086	H7	0.113
H8	0.102	H8	0.105
H9	0.102	H9	0.105
H10	0.086	H10	0.113
O11	-0.392	O11	-0.389
H12	0.259	H12	0.260
H13	0.082	F13	-0.291

Table S2: Atomic dipoles for PhOH and F-PhOH from fitting to the molecular electrostatic potential.¹ Q_{xx} are the spherical MTP coefficients expressed in the local axis system.

Atom	Q10 (e)	Q11c (e)	Q11s (e)
PhOH			
C1	-0.015	0.0	0.033
C2	-0.016	-	0.030
C3	-0.0002	-	0.054
C4	0.028	0.0	0.089
C5	-0.0002	-	0.054
C6	-0.016	-	0.030
O11	0.0	0.099	-0.070
H13	0.0	0.0	0.0
F-PhOH			
C1	-0.011	0.0	0.180
C2	-0.022	-	0.073
C3	-0.025	-	0.017
C4	0.015	0.0	0.122
C5	-0.025	-	0.017
C6	-0.022	-	0.073
O11	0.0	0.121	-0.140
F13	0.147	0.0	0.008

Table S3: Atomic quadrupoles for PhOH and F-PhOH from fitting to the molecular electrostatic potential.¹ Q_{xx} are the spherical MTP coefficients expressed in the local axis system.

Atom	Q20 (<i>e</i>)	Q21c (<i>e</i>)	Q21s (<i>e</i>)	Q22c(<i>e</i>)	Q22s(<i>e</i>)
PhOH					
C1	-0.029	0.0	0.001	-0.005	0.0
C2	-0.026	-	-0.0003	-0.0013	-
C3	-0.012	-	0.002	0.0039	-
C4	8.04×10^{-5}	0.0	0.013	0.0015	0.0
C5	-0.012	-	0.0029	0.0039	-
C6	-0.0260	-	-0.0003	-0.0013	-
O11	-0.006	0.0	0.0	0.015	-0.0278
H13	0.0	0.0	0.0	0.0	0.0
F-PhOH					
C1	-0.024	0.0	0.006	-0.007	0.0
C2	-0.042	-	0.003	0.0005	-
C3	-0.029	-	0.002	0.009	-
C4	0.005	0.0	0.022	-0.009	0.0
C5	-0.029	-	0.002	0.009	-
C6	-0.042	-	0.003	0.0005	-
O11	-0.034	0.0	0.0	0.029	-0.0798
F13	-0.034	0.0	0.0016	0.009	0.0

Table S4: The frequency maxima obtained from frequency distribution, power and IR spectrum using PC/MTP model in the gas phase and solvent for five different modes in the frequency range of 1100 to 1400 cm^{-1} .

Mode	MD							
	$P(\omega)$		PS(CF)		PS(CF)		IR(CF)	
	MTP _{gas}	MTP _{H₂O}	MTP _{gas}	MTP _{H₂O}	PC _{gas}	PC _{H₂O}	PC _{H₂O}	MTP _{H₂O}
ν_1	1140	1149	1141	1158	1140	1163	1148	1151
ν_2	1170	1172	1170	1185	1171	1184	1172	1174
ν_3	1225	1236/1251	1227	1248	1226	1265	1243	1249
ν_4	1286	1294	1285	1305	1286	1310	1294	1296
ν_5	1324	1330	1324	1345	1324	1343	1331	1333

Table S5: Parameters obtained from fitting the FFCE to Eq. 3 based on frequencies from INM using 5 ns MTP (10^6 snapshots) simulation of F-PhOH in H_2O . Average frequency $\langle\omega\rangle$ of the asymmetric stretch in cm^{-1} , the amplitudes a_1 and a_2 in ps^{-2} , the decay times τ_1 and τ_2 in ps, and the offset Δ_0 in ps^{-2} . The FFCE for the OH-stretch is reported in Figure S10.

Mode	$\langle\omega\rangle$	a_1	τ_1	a_2	τ_2	Δ_0
ν_1	1149.71	0.36	0.08	0.06	0.45	0.0005
ν_2	1173.00	0.29	0.05	0.04	0.38	0.0003
ν_3	1248.40	2.31	0.10	0.32	0.60	0.0095
ν_4	1295.18	0.68	0.08	0.14	0.28	0.0029
ν_5	1332.04	1.01	0.09	0.06	0.83	0.0055
OH	3500.22	32.11	0.10	17.72	0.50	0.19

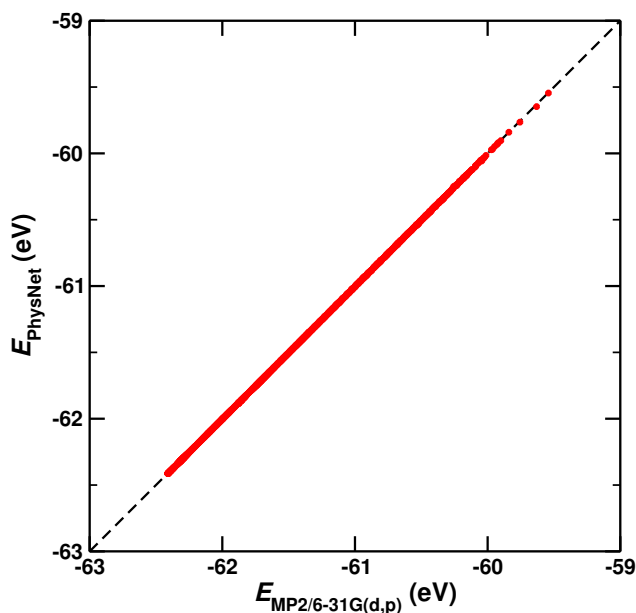


Figure S1: Correlation between the ab initio and PhysNet energies for a set of 3700 randomly selected points averaged over 980/982 trajectories with $R^2 = 0.9999$ and a root mean square error of 0.0037 eV.

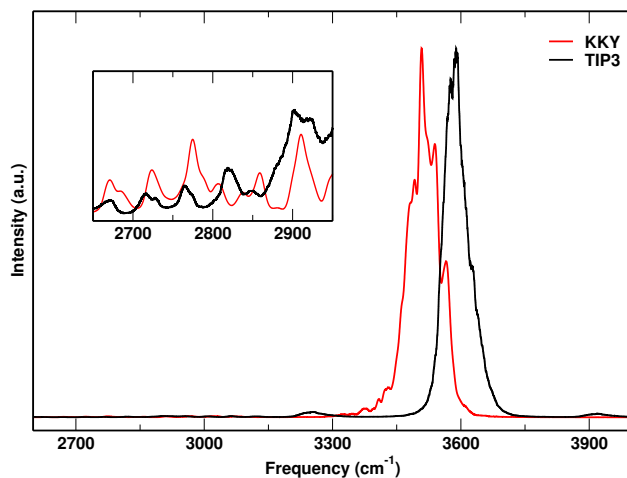


Figure S2: The power spectrum for the phenol-OH stretching vibration from a 5 ns simulation of F-PhOH with flexible (red) KKY water²⁻⁴ compared to TIP3 (black) model. The red shift from the simulations with KKY is -78 cm^{-1} .

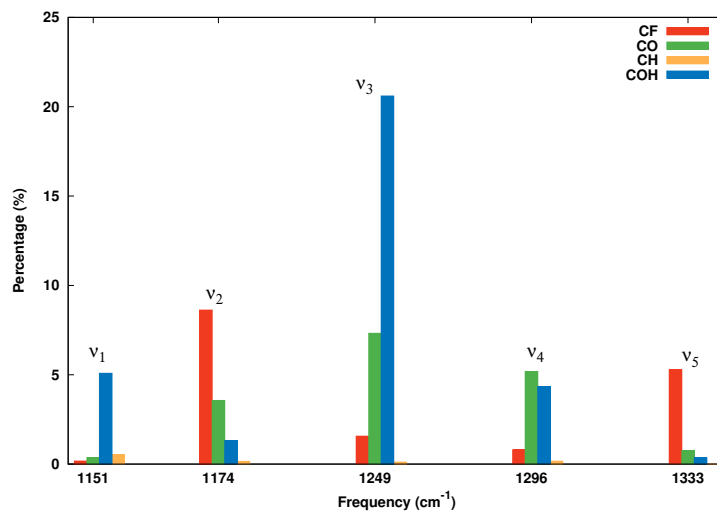


Figure S3: Participation ratio of the CF (red), CO (green), and CH (orange) stretching and the COH bending (blue) motions to the 5 modes between 1140 and 1350 cm^{-1} by using the “project” facility in CHARMM for 10^5 snapshots from the MTP simulation of F-PhOH in H_2O . The remaining contributions are from low frequency modes.

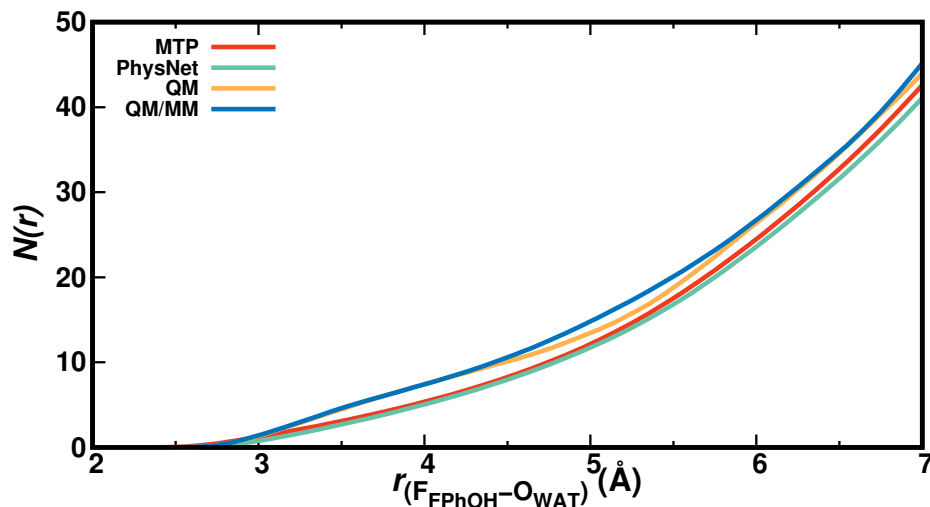


Figure S4: The total number of water molecules within distance r of the fluorine atom for the MTP (red), PhysNet (green), QM/MM (orange) and QM (blue) simulations.

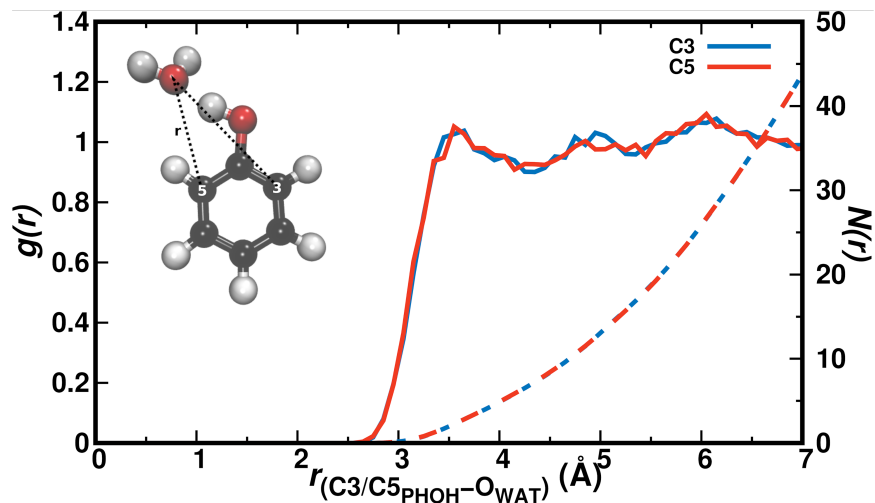


Figure S5: The radial distribution function between the water-oxygen atoms and the two carbon atoms flanking the COH group in PhOH from a 5 ns simulation with MTP. It is demonstrated that the solvent distribution is converged. Comparison with the red trace in Figure 4A indicates that hydration around the CF and CH groups is similar with the first maximum at a similar C-O_W separation.

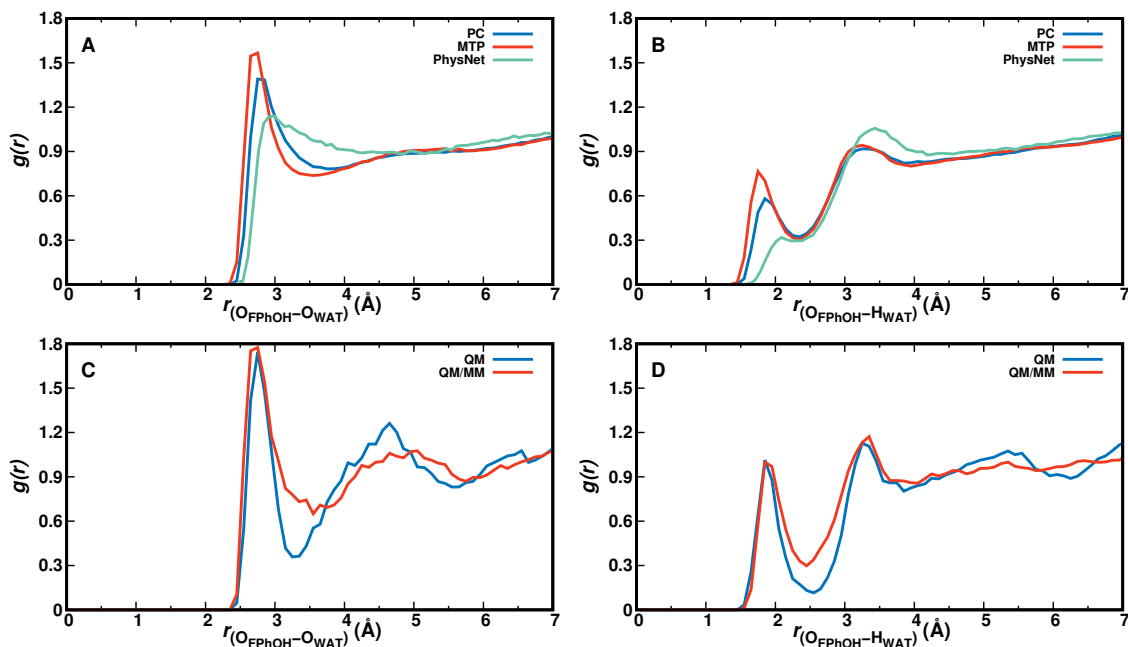


Figure S6: The $g(r)$ for A) $O_{\text{FPhOH}}-O_{\text{WAT}}$ and B) $O_{\text{FPhOH}}-H_{\text{WAT}}$ distances as obtained from PC (blue), MTP (red) and PhysNet (green) simulations of F-PhOH in H_2O . Panel C and D from QM and QM/MM simulations.

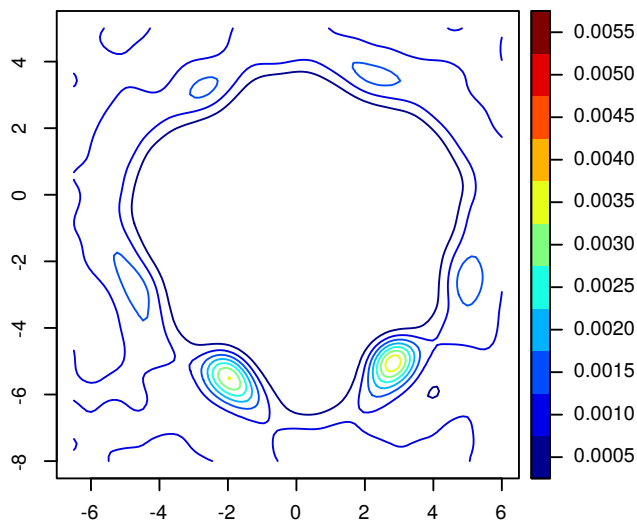


Figure S7: 2d-distribution from MTP simulations with TIP3P water. The structures are re-oriented with reference to the solute heavy atoms, but excluding the phenolic-oxygen atom. This differs from the selection used in Figure 6 and allows to visualize the symmetric distribution of the solvent water molecules around the $-\text{COH}$ group.

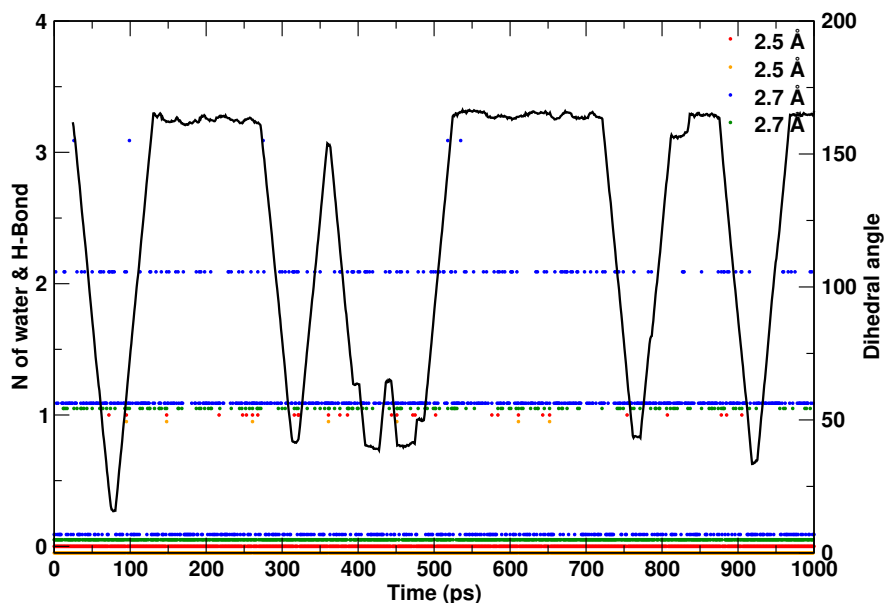


Figure S8: Dihedral rotation of the CCOH angle together with the water occupation of the -OH group (circles) and number of H-bonds (crosses) for $O_{\text{COH}}-O_{\text{W}}$ separations of a) 2.5 Å (red & orange) and b) 2.7 Å (blue & green). With the shorter cutoff there is no water molecule hydrogen bonded to the rotatable COH group for most of the simulation time and occasionally one water is sufficiently close to form an H-bond. For the longer cutoff water presence is frequent and H-bonding (green crosses) is more prevalent. The alteration between H-bonded and non-H-bonded -COH group explains the spectroscopy seen in Figure S2. A direct correlation between rotation of the CCOH angle and water occupation can not be established convincingly although it is likely that rotation of the COH group requires water to detach from it. The dihedral time series is locally averaged over a time window of 50 ps. Simulations with ML/MM MD yield a comparable time series with transitions on the ~ 100 ps time scale.

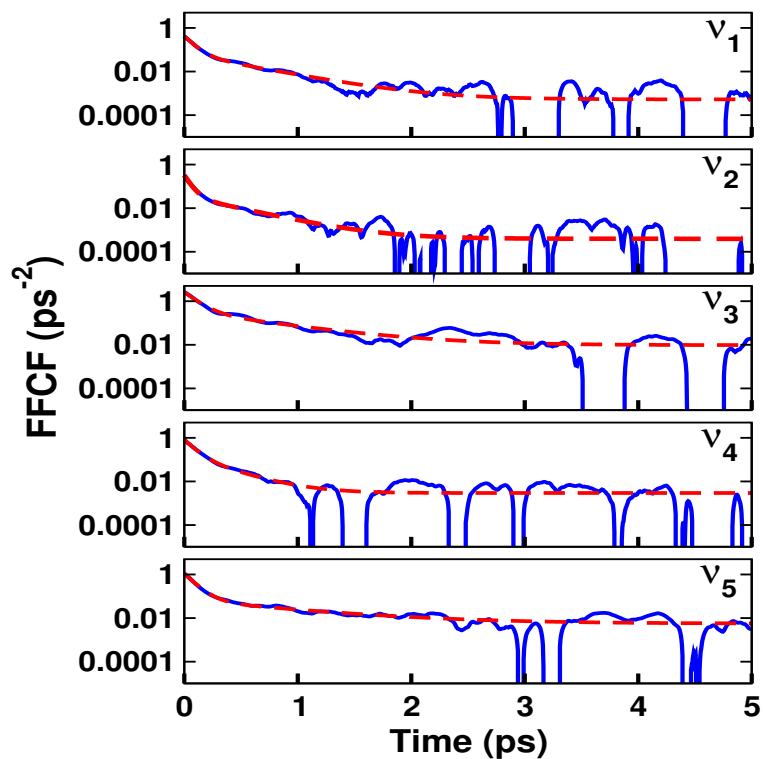


Figure S9: FFCFs from INM frequency calculations for F-PhOH in water from a 5 ns simulation using MTP. The FFCFs for the 5 modes ν_1 to ν_5 between 1100 and 1400 cm⁻¹ are reported. The solid lines are the raw FFCF data and the dashed lines show the corresponding fit with fitting parameters reported in Table S5. Logarithmic scale is chosen for the y -axis.

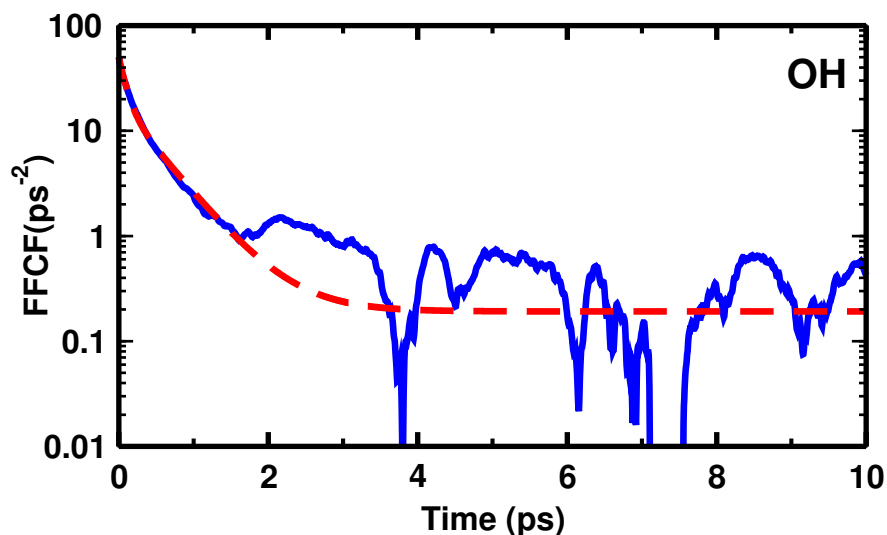


Figure S10: FFCFs from INM frequency calculations for F-PhOH in water from a 5 ns simulation using MTP. The FFCFs for the OH mode is reported. The solid lines are the raw FFCF data and the dashed lines show the corresponding fit with fitting parameters reported in Table 2. Logarithmic scale is chosen for the y -axis.

References

- (1) Hedin, F.; El Hage, K.; Meuwly, M. A Toolkit to Fit Nonbonded Parameters from and for Condensed Phase Simulations. *J. Chem. Theo. Comp.* **2016**, *56*, 1479–1489.
- (2) Burnham, C. J.; Li, J. C.; Leslie, M. Molecular Dynamics Calculations for Ice Ih. *J. Phys. Chem. B* **1997**, *101*, 6192–6195.
- (3) Plattner, N.; Meuwly, M. Atomistic Simulations of CO Vibrations in Ices Relevant to Astrochemistry. *ChemPhysChem* **2008**, *9*, 1271–1277.
- (4) Kumagai, N.; Kawamura, K.; Yokokawa, T. An Interatomic Potential Model for H₂O: Applications to Water and Ice Polymorphs. *Mol. Sim.* **1994**, *12*, 177–186.